Structure of Calcineurin bound to PI4KA reveals dual interface in both PI4KA and FAM126A

Alexandria L Shaw[1,2]*, Sushant Suresh[2]*, Matthew AH Parson[2], Noah J Harris[2], Meredith L Jenkins[2], Calvin K Yip[1], John E Burke[1,2#]

[1] Department of Biochemistry and Molecular Biology, The University of British Columbia, Vancouver, British Columbia V6T 1Z3, Canada

[2] Department of Biochemistry and Microbiology, University of Victoria, Victoria, BC, V8W 2Y2, Canada

* These authors contributed equally

[#] Lead contact: John E Burke, jeburke@uvic.ca

Running title: Structure of PI4KA-Calcineurin interface

Abstract

Phosphatidylinositol 4 kinase alpha (PI4KA, or PI4KIIIα), is crucial for maintaining the PI4P and phosphatidylserine pools of the plasma membrane. A key regulator of PI4KA is its association into a trimeric complex with TTC7 and FAM126 regulatory proteins. The activity of this complex can be regulated by the lipidated CNAβ1 isoform of the protein phosphatase Calcineurin. We previously identified that CNAβ1 directly binds to FAM126A. Here, we report a cryo-EM structure of a truncated PI4KA complex bound to Calcineurin, which reveals a direct Calcineurin interaction with PI4KA, forming a dimer of pentamers (PI4KA-TTC7B-FAM126A-CNA-CNB). HDX-MS, cryo-EM and computational modelling show that Calcineurin forms a direct complex with evolutionarily conserved IKISVT and LVPP sequences in PI4KA's horn and dimerization domains. We also characterised conserved LTLT and PSISIT Calcineurin binding sequences in the C-terminus of FAM126A. These sites are located in close spatial proximity to multiple phosphorylation sites in the PI4KA complex, suggesting key roles of Calcineurin-regulated phosphosites in PI4KA regulation. This work reveals novel insight into how Calcineurin can regulate PI4KA activity at the plasma membrane.

30

31 **Introduction**

32 Phosphoinositide lipids act as master second messengers which regulate myriad
33 cellular processes (Hammond & Burke, 2020; Balla, 2013; Burke *et al*, 2023). The
34 precursor of all phosphoinositides is the lipid phosphatidylinositol (PI), with one of the
35 most abundant phosphoinositides being phosphatidylinositol 4-phosphate (PI4P). PI4P is
36 found in the cell in various subcellular membrane locations, including the Golgi, the endo-
37 lysosomal system, and the plasma membrane (PM) (Batrouni & Baskin, 2021). PI4P is
38 generated by the action of four different phosphatidylinositol 4-kinases (Boura & Nencka,
39 2015; Dornan *et al*, 2016), with the plasma membrane pool being primarily generated by
40 type III phosphatidylinositol 4-kinase alpha (PI4KIIIα, which will be referred to by its gene
41 name *PI4KA* for the remainder of the manuscript). The generation of PI4P by PI4KA at
42 the plasma membrane is essential for the generation of membrane asymmetry, partially
43 through its critical role in controlling phosphatidylserine transport to the plasma
44 membrane (Chung *et al*, 2015).

45 PI4KA is a multi-domain protein, composed of an alpha-solenoid (horn) domain, a
46 dimerization domain, a helical domain, and a bi-lobal kinase domain (Lees *et al*, 2017). It
47 is functional as a large multi-protein complex, primarily associated with two scaffolding
48 proteins, TTC7 (with two possible isoforms TTC7A or TTC7B) and FAM126 (with two
49 possible isoforms FAM126A or FAM126B) (Dornan *et al*, 2018; Baskin *et al*, 2016; Lees
50 *et al*, 2017). PI4KA and TTC7 are highly conserved throughout all eukaryotes, with
51 FAM126 being lost in many simple unicellular eukaryotes (Suresh & Burke, 2023; Baird
52 *et al*, 2008). The PI4KA-TTC7-FAM126 complex forms a dimer of trimers, with TTC7 and
53 FAM126 stabilizing PI4KA, which together will be referred to as the PI4KA complex for
54 the remainder of the manuscript (Lees *et al*, 2017; Baskin *et al*, 2016; Dornan *et al*, 2018).
55 Functionally, PI4KA is recruited to the membrane by a palmitoylated EFR3 protein (with
56 two possible isoforms EFR3A/EFR3B (Nakatsu *et al*, 2012). The exact binding site of
57 EFR3 to the PI4KA complex is not fully resolved but putatively involves an evolutionarily
58 conserved C-terminal region of TTC7 (Wu *et al*, 2014). PI4KA faces a complicated
59 challenge in the generation of PI4P at the plasma membrane, as its substrate PI is present

at only trace levels (Zewe *et al*, 2020; Pemberton *et al*, 2020), with the exact mechanism of how PI4KA is regulated and activated at the plasma membrane still not fully understood.

PI4KA, TTC7, FAM126, and its accessory proteins are implicated in myriad human diseases. Intriguingly, both the loss-of-function and gain-of-function of PI4KA can be drivers of human disease (Barlow-Busch *et al*, 2023). Down-regulation of PI4KA signaling is observed in intestinal atresia driven by mutations in TTC7A (Bigorgne *et al*, 2014), hypomyelination and congenital cataracts by a deficiency in FAM126A (Zara *et al*, 2006), and neurological, intestinal and immunological diseases caused by loss-of-function mutations in PI4KA (Salter *et al*, 2021; Verdura *et al*, 2021).

One of the recently discovered regulators of PI4KA signaling is the protein phosphatase Calcineurin, which is a ubiquitously expressed serine/threonine phosphatase activated by Ca^{2+} signaling (Ulengin-Talkish & Cyert, 2023). Calcineurin is composed of two subunits, calcineurin A (CNA) and calcineurin B (CNB), with multiple isoforms of each subunit. We have found that the lipidated CNAβ1 isoform of Calcineurin is a direct regulator of PI4KA signaling, and upon palmitoylation is recruited to the PM (Ulengin-Talkish *et al*, 2021). Cellular studies have shown that Calcineurin inhibition causes reduced PI4P synthesis following hormone-mediated $PI(4,5)P_2$ depletion, and we identified a short linear PxIxIT motif (SLiM) in FAM126A that mediates binding to CNAβ1 (Ulengin-Talkish *et al*, 2021).

To fully explore the molecular mechanisms of how Calcineurin can bind to and regulate the PI4KA complex we have utilised a synergistic application of cryo-EM, HDX-MS, and AlphaFold modelling. Our cryo-EM structure reveals that Calcineurin not only binds the FAM126A disordered tail but also forms an evolutionarily conserved interface with the horn region of PI4KA, which interacts with the CNA binding site for PxIxIT motifs. This interface was validated by both HDX-MS and AlphaFold-Multimer modelling. This map also had increased local resolution in the horn compared to previous cryo-EM analysis allowing for the building of a complete model of the PI4KA horn, as well as the interface between TTC7B and the N-terminus of the PI4KA horn. HDX-MS also revealed an LVPP sequence in a disordered region of PI4KA's dimerization domain, which could

interact with CNB's LxVP binding motif. These evolutionarily conserved PI4KA Calcineurin SLiM motifs orient the active site of Calcineurin near multiple evolutionarily conserved phosphorylation sites of unknown function. Overall, our findings provide useful insight into the molecular and structural basis of PI4KA complex regulation by CNAβ1 at the plasma membrane.

Results and Discussion

Cryo-EM structure of the PI4KA*-Calcineurin *complex

We purified the human PI4KA complex with a truncated FAM126A tail (full-length PI4KA/TTC7B and truncated FAM126A (aa 1-308), referred to in the rest of the manuscript as PI4KA complex (Fig 1A). This construct lacks the FAM126A C-terminus, which was previously identified as a binding site for Calcineurin (composed of a dimer of CNA and CNB subunits). We had previously observed a change in protein dynamics in the horn region of PI4KA in full-length PI4KA-TTC7B-FAM126A upon binding Calcineurin (Ulengin-Talkish *et al*, 2021), and it was unknown if this was driven by allosteric conformational changes or acted as a direct Calcineurin binding interface. To further investigate this, we purified the Calcineurin heterodimer (alpha isoform of CNA with CNB) to conduct structural studies of the PI4KA-Calcineurin interaction. This was done as all Calcineurin isoforms interact with their substrates through the same mechanism(s) and the alpha isoform of CNA is best behaved in solution and therefore more suitable for *in vitro* structural studies.

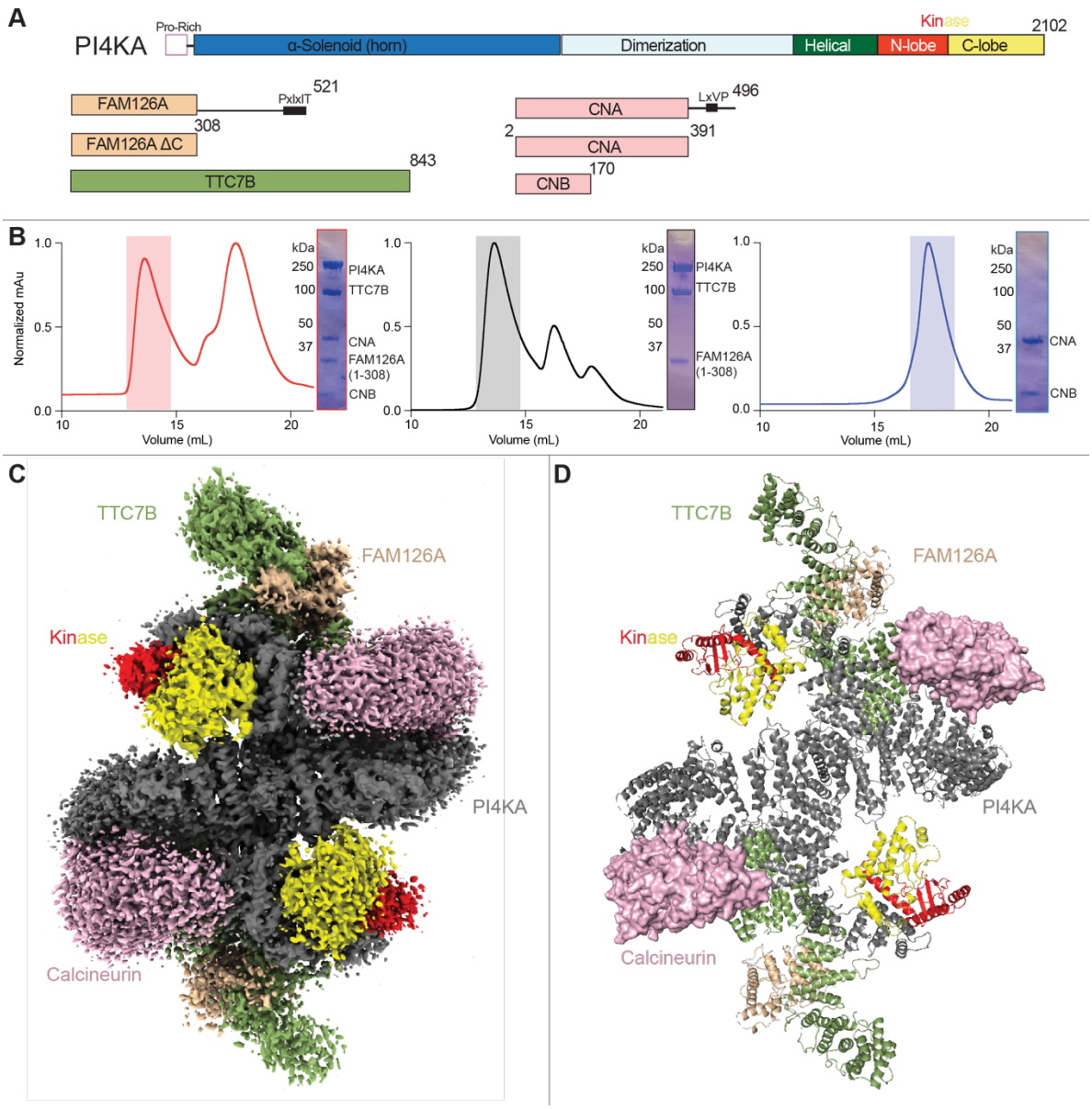

Figure 1. Calcineurin forms a complex with the PI4KA complex (see supplemental figures 1-3)

A. Domain schematics of catalytic PI4KA, regulatory proteins TTC7B and FAM126A (Full length and truncated, FAM126A ΔC used in all experiments) and the serine/threonine phosphatase Calcineurin (heterodimer of CNA (top: Full length β1 isoform, bottom: truncated α1 isoform used in all experiments), and CNB).

B. Gel filtration elution profiles of PI4KA complex apo (black), Calcineurin apo (blue), or PI4KA complex bound to Calcineurin (red). SDS-polyacrylamide gel electrophoresis image of specified peaks.

C. Cryo-EM density map of the PI4KA complex bound to Calcineurin.

D. Cartoon/surface representation of the PI4KA complex bound to Calcineurin coloured according to the in-figure text legend.

122 To validate if the PI4KA complex could directly interact with Calcineurin in the
123 absence of the C-terminus of FAM126A, we analysed three complexes by gel filtration:
124 PI4KA complex, Calcineurin, and the co-complex. Elution profiles were consistent with
125 the formation of a stable stochiometric dimer of pentamers (pentamer composed of
126 PI4KA, TTC7B, FAM126A ΔC, CNA, and CNB, Fig. 1B). To delineate the molecular basis
127 for how Calcineurin binds to PI4KA we examined the architecture using an approach
128 combining cryo-EM, hydrogen deuterium exchange mass spectrometry (HDX-MS), and
129 AlphaFold-Multimer modelling.
130 We first conducted cryo-EM analysis of the PI4KA complex bound to Calcineurin.
131 Although negative stain analysis revealed that the purified PI4KA complex bound to
132 Calcineurin was homogeneous and we could generate high-quality vitrified specimens,
133 our initial attempts to obtain good 3D reconstructions were unsuccessful due to preferred
134 particle orientation. We reasoned that this could likely be due to the dynamic nature of
135 Calcineurin relative to PI4KA, and PI4KA's proposed membrane binding interface leading
136 to the accumulation of PI4KA at the air-water interface. To obtain a more "rigid" complex
137 for cryo-EM analysis, we treated the PI4KA complex bound to Calcineurin with BS^3
138 crosslinker, followed by gel filtration to remove aggregate proteins. Analysis of this
139 complex allowed for the refinement of ~235,760 particles leading to a 3D reconstruction
140 at a nominal resolution of 3.51 Å (Fig 1C, Fig S1). There was a difference in local
141 resolution between the two dimers of pentamers (Fig. S1C). For this reason, we have
142 focused our molecular analysis on the interaction between Calcineurin/PI4KA, and
143 PI4KA/TTC7B on the higher local resolution pentamer. The density map was of sufficient
144 quality to allow for automated and manual building of the majority of the PI4KA subunit,
145 with a clear orientation of the available cryo-EM and X-ray crystallography models of
146 TTC7B-FAM126A in the electron density (Wu *et al*, 2014; Lees *et al*, 2017). The regions
147 with the lowest local resolution correspond to the two Calcineurin molecules. Despite this,
148 the orientation of Calcineurin in the density was unambiguous, and we could
149 unambiguously define this interface using AlphaFold modelling and HDX-MS (described
150 further below).

151 Our cryo-EM map captures more details in PI4KA than compared to the previously
152 reported cryo-EM structure of the PI4KA complex (Lees *et al*, 2017). Using a combination
153 of manual model building and AlphaFold/trRosetta modelling of specific regions (Jumper
154 *et al*, 2021; Baek *et al*, 2021) we were able to confidently build an additional ~700 residues
155 of PI4KA corresponding to the solenoid α helices in the horn domain (Fig S2, S3).
156 Intriguingly, the solenoid horn domain showed a slight deviation compared to the previous
157 cryo-EM structure of PI4KA (Fig S2B). It is not known if this conformational difference
158 was driven by the interaction with Calcineurin or by the chemical crosslinker used to
159 stabilize the assembly. The local resolution of the contact between the N-terminus of
160 PI4KA and TTC7B allowed for unambiguous determination of the residues mediating this
161 interface (Fig 2, S1C, S2C). The interface between the N-terminus of the horn domain
162 (composed of solenoid α helices 1+2 [residues 31-59], Fig 2C) and the C-terminus of
163 TTC7B was evolutionarily conserved through *C. elegans* (Fig 2D), while only weakly
164 conserved in yeast. It has been previously shown that disease-linked C-terminal
165 truncations in TTC7A that disrupt this interface can still bind to PI4KA, although they show
166 decreased PI4KA activity (Lees *et al*, 2017). Studies on PI4KA were initially complicated
167 by improper annotation of the N-terminal start site (ORF starting at M59) (Nakatsu *et al*,
168 2012), with our results revealing the molecular basis for why the two evolutionarily
169 conserved N-terminal PI4KA helices immediately before this site are critical in mediating
170 contact with the C-terminus of TTC7. This further reinforces that any cellular studies
171 examining PI4KA's roles with a construct containing the improperly annotated start site
172 should be interpreted with extreme caution.

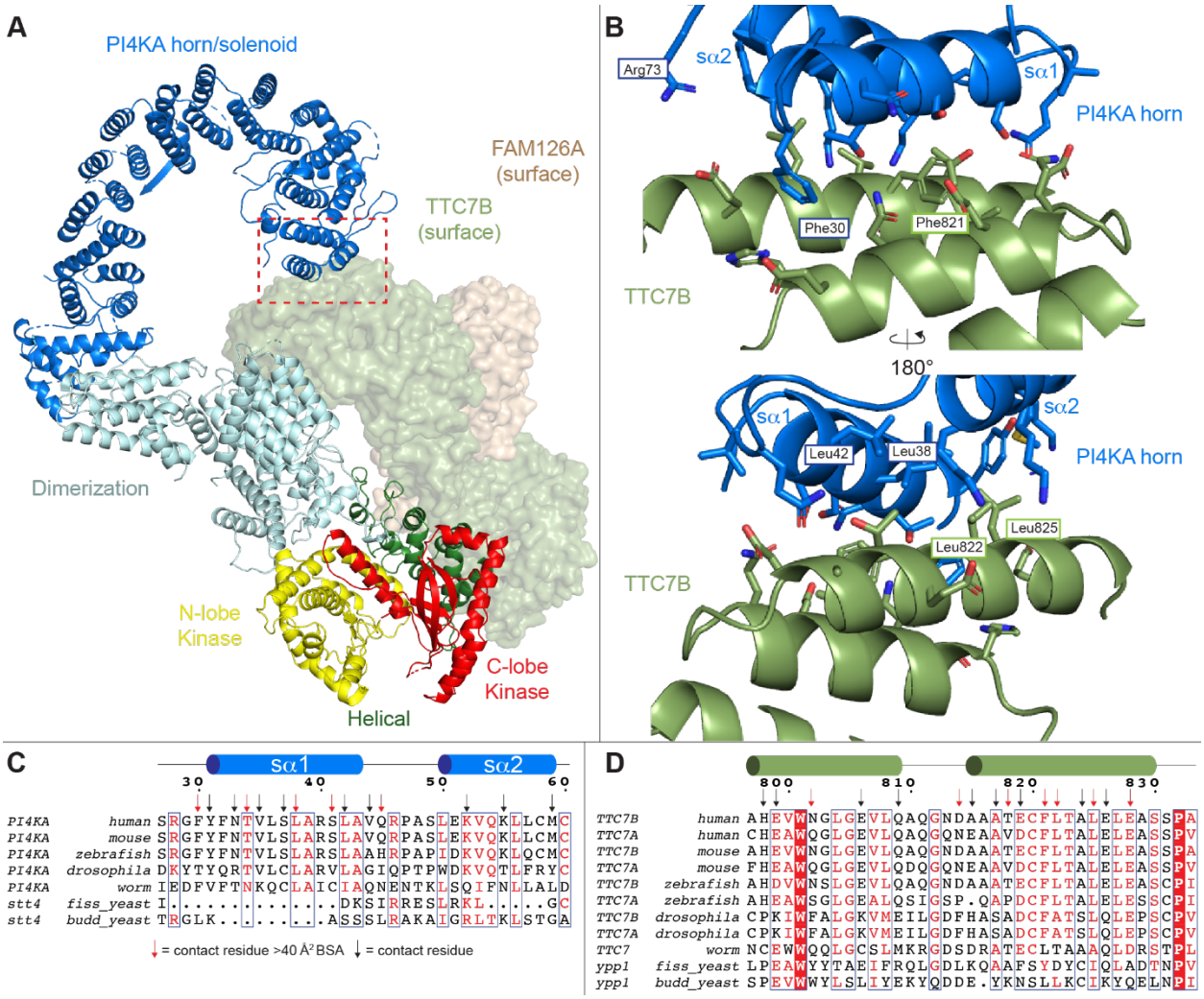

Figure 2. The N-terminus of the PI4KA solenoid interacts with the TTC7B C-terminal region

A. Cartoon representation of an isolated PI4KA/TTC7B/FAM126A trimer. PI4KA is shown as a cartoon with individual domains coloured according to the in-figure text. TTC7B and FAM126A are shown as surfaces coloured according to the in-figure text. Red box depicts the PI4KA solenoid-TTC7B interface.

B. Cartoon representation of the PI4KA solenoid-TTC7B interaction interface. Side chains are shown for residues within 6 Å of either interface, which are either annotated on the cartoon or in panel C/D. Annotated residues on the cartoon were chosen to provide readers with a point of reference.

C. Multiple sequence alignment of PI4KA from *Homo sapiens, Mus musculus, Danio rerio, Drosophila melanogaster, Caenorhabditis elegans*, *Schizosaccharomyces pombe,* and *Saccharomyces cerevisiae.* sα1 and sα2 are annotated above the alignment. Residues within 6 Å shown in panel B are annotated using arrows, with red arrows indicating a BSA of > 40 Å^2.

D. Multiple sequence alignment of TTC7A/B from *Homo sapiens, Mus musculus, Danio rerio, Drosophila melanogaster, Caenorhabditis elegans*, *Schizosaccharomyces pombe,* and *Saccharomyces cerevisiae.* TTC7B secondary structure observed from experimental data is annotated above the alignment. Residues within 6 Å shown in panel B are annotated using arrows, with red arrows indicating a BSA of > 40 Å^2.

189

190 **Cryo-EM, HDX-MS, and AlphaFold analysis of PI4KA-Calcineurin binding site**

191 The local resolution of Calcineurin allowed us to fit previously solved structures of
192 Calcineurin into the density (Hendus-Altenburger *et al*, 2019), however, it was not
193 sufficient to model the exact PI4KA residues mediating binding. To precisely map the
194 location of the Calcineurin binding site we utilised hydrogen deuterium exchange mass
195 spectrometry (HDX-MS), which is a technique used to investigate protein dynamics and
196 is useful when investigating protein-protein interfaces (Masson *et al*, 2017; Stariha *et al*,
197 2021; Parson *et al*, 2022). The rate at which deuterium is exchanged on the amide
198 backbone is dependent on the stability of protein secondary structure, temperature, and
199 pH. Deuterium incorporation is localised at peptide-level resolution through the generation
200 of pepsin-generated peptides.

201 HDX-MS experiments compared the dynamics of Calcineurin and the PI4KA
202 complex both free in solution and when in the co-complex. Initial experiments were carried
203 out at a high concentration of PI4KA complex and Calcineurin (1.3 μM final) at a 1:1 ratio
204 to promote binding of the weak complex, with deuterium incorporation measured over
205 three time points (3, 30, 300 s at 18°C at pH 7.0). These experiments were carried out
206 under three conditions: Calcineurin apo, PI4KA complex apo, and the co-complex,
207 allowing us to map changes on both sides of the interface. These experiments revealed
208 that the interacting sites in PI4KA were all in regions that were disordered, consistent with
209 the biophysical properties of the motifs that mediate interaction(s) with Calcineurin. To
210 better cover the deuterium incorporation of these highly dynamic regions we carried out
211 an additional experiment using a pH and temperature regime optimized for disordered
212 regions (pH 6.5, 0°C) (Coales *et al*, 2010). Experiments were carried out with a 1:2 ratio
213 of the PI4KA complex to Calcineurin (1.25 and 2.5 μM final), with deuterium incorporation
214 measured over three time points (3, 10, 30 s). The full raw deuterium incorporation data
215 for all HDX-MS experiments are provided in the source data. Coverage of all proteins was
216 over 85%, with all HDX-MS processing statistics available in the source data.

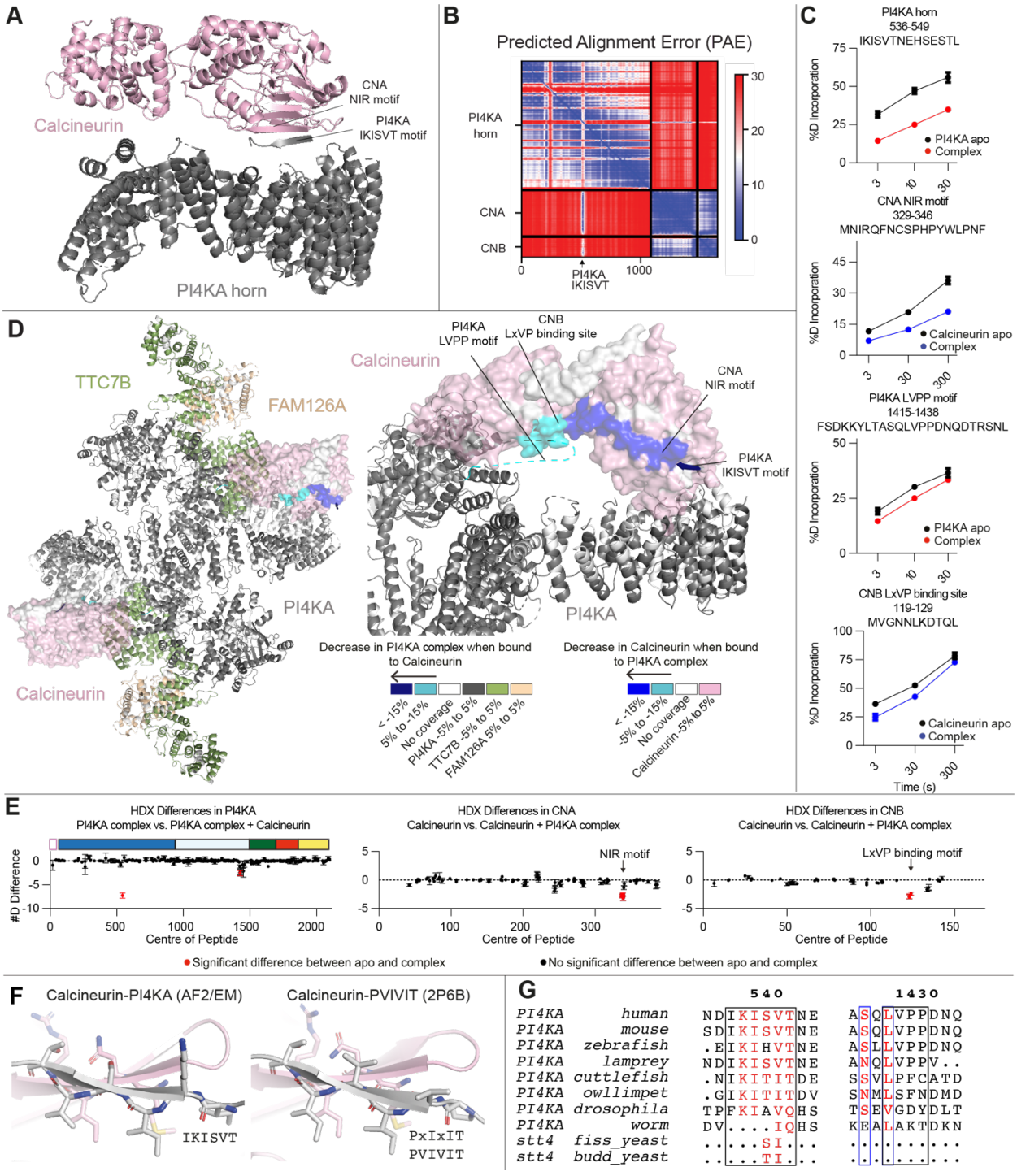

Figure 3. Calcineurin interacts with the PI4KA solenoid

A. AlphaFold-Multimer model of the PI4KA horn in complex with Calcineurin with the per-residue confidence metric predicted local-distance difference test (pLDDT) <60 removed.

B. Predicted aligned error (PAE) of the AlphaFold-Multimer prediction of the PI4KA horn and Calcineurin.

222 **C.** Selected deuterium exchange time courses of PI4KA (pH 6.5, 0°C) and Calcineurin (pH 7.0, 18°C)
223 peptides that showed significant decreases in exchange upon complex formation. Error is shown as
224 standard deviation (SD) (n=3).
225 **D.** (L) PI4KA complex (pH 6.5, 0°C) peptides showing significant differences in deuterium exchange
226 (defined as >5%, 0.45 Da, and p>0.01 in an unpaired two-tailed t test at any time point) upon complex
227 formation, and Calcineurin (pH 7.0, 18°C) peptides showing significant differences in deuterium exchange
228 (defined as >5%, 0.45 Da, and p>0.01 in an unpaired two tailed t-test at any time point) upon complex
229 formation. Differences are mapped on the structural model, with a disordered loop showing changes in
230 HDX being represented by a dotted line. Differences are indicated by the legend. (R) Differences are
231 mapped on a zoomed in structural model of the interface. Differences are indicated by the legend in A.
232 **E.** Sum of the number of deuteron difference of (L) PI4KA upon complex formation with Calcineurin (pH
233 6.5, 0°C), (M) Calcineurin A or (R) Calcineurin B upon complex formation with the PI4KA complex (pH
234 7.0,18°C), analysed over the entire deuterium exchange time course for PI4KA complex/Calcineurin. (M/R)
235 Each point is representative of the centre residue of an individual peptide. Peptides that met the significance
236 criteria described in panel D are coloured red. Error is shown as the sum of standard deviations across all
237 3 time points (SD) (n=3).
238 **F.** Cartoon representation of the (L) IKISVT mediated interaction with Calcineurin's NIR motif and (R)
239 canonical PxIxIT mediated interaction with Calcineurin's NIR motif.
240 **G.** Multiple sequence alignment of PI4KA from *Homo sapiens, Mus musculus, Danio rerio, Petromyzon*
241 *marinus, Sepia pharaonis, Lottia gigantea, Drosophila melanogaster, Caenorhabditis elegans*,
242 *Schizosaccharomyces pombe,* and *Saccharomyces cerevisiae,* showing conservation of the PI4KA IKISVT
243 and LVPP motifs.
244
245 We observed a significant decrease (significant change defined as greater than
246 both 5% and 0.45 Da at any time point in any peptide with an unpaired two-tailed t test
247 p<0.01) in deuterium exchange at residues 331-347 (NIR binding site) in CNA, residues
248 119-129 (LxVP binding pocket) in CNB, and residues 538-549 and 1424-1438 in PI4KA.
249 The 538-549 region is an unstructured region between solenoid α helices 17 and 18 (Fig
250 3C-E, S4). This is similar to decreases in exchange observed when using full length
251 PI4KA complex (Ulengin-Talkish *et al*, 2021), however the absence of the FAM126A C-
252 terminus allows for a confident validation of a protein-protein interface. An additional
253 previously undescribed decrease in exchange was observed in PI4KA at residues 1417-

254 1438, which covers a disordered region containing an LVPP sequence, with this exact
255 sequence being previously found to bind to CNB's LxVP binding pocket (Li *et al*, 2020).
256 Having experimentally identified and validated the binding interface between
257 Calcineurin and PI4KA, we carried out AlphaFold-Multimer analysis to predict the
258 molecular details of this interaction. Based on our initial HDX-MS results we carried out
259 searches composed of Calcineurin along with the entire PI4KA horn domain, as well as
260 a region containing residues 400-1500. In both cases, AlphaFold-Multimer predicted a
261 single beta strand (residues 536-541 containing the IKISVT sequence) in PI4KA binding
262 to the NIR region of Calcineurin that mediates binding to PxIxIT motifs, with predicted
263 alignment error (PAE) scores consistent with a stable interface (Fig. 3A-B). The top-
264 ranked predicted structural model had overall high pLDDT scores, with high confidence
265 (pLDDT >70) for IKISVT binding to Calcineurin. Although there was no interaction
266 predicted with the LVPP sequence, this region was in close spatial proximity to CNB in
267 these models. There were no other predicted interactions between PI4KA and
268 Calcineurin, consistent with the HDX-MS analysis and the low local resolution of
269 Calcineurin in the cryo-EM density. The binding position of IKISVT bound to the NIR
270 region of Calcineurin is consistent with Calcineurin binding to the canonical PxIxIT
271 docking groove (Fig. 3F), and is also consistent with the high degree of plasticity observed
272 in Calcineurin SLiM motifs (Brauer *et al*, 2019; Wigington *et al*, 2020). The IKISVT and
273 LVPP binding sites for Calcineurin in PI4KA were evolutionarily conserved throughout all
274 vertebrates, with them being conserved in chordates, and lost in arthropods (Fig. 3G).
275
276 **Comparison of the FAM126A-Calcineurin and PI4KA-Calcineurin binding sites**
277 To fully understand the myriad molecular interactions mediating how the PI4KA
278 complex interacts with Calcineurin, we wanted to determine how the C-terminus of
279 FAM126A, which is absent from our cryo-EM structure, might interact with Calcineurin.
280 To investigate this interaction, we purified the FAM126A C-terminus [FAM126A (415-
281 521)] and used HDX-MS to compare the dynamics of FAM126A (415-521) apo to
282 FAM126A (415-521) in complex with Calcineurin (Fig. 4, S4). The full raw deuterium
283 incorporation data for all HDX-MS experiments are provided in the Source Data.

284 The HDX-MS experiments were carried out at a 1:1 ratio, with deuterium
285 incorporation measured over three time points (3, 30, 300 s at 0°C). As the C-terminus of
286 FAM126A is intrinsically disordered in the absence of binding partners (Fig 4A), we
287 carried out HDX-MS experiments at a temperature of 0°C and a pH of 6.5 to optimize the
288 experiment for rapidly exchanging amide hydrogens (Coales *et al*, 2010). Two areas in
289 FAM126A (415-521) had significant changes in deuterium exchange upon complex
290 formation with Calcineurin (significant change defined as greater than both 5% and 0.45
291 Da at any time point in any peptide with an unpaired two-tailed t test $p<0.01$). As expected,
292 the largest significant decrease in deuterium exchange occurred in peptides containing
293 the PSISIT binding site (494-521) (Fig. 4D-F). Another site with a significant decrease in
294 deuterium contained an LTLT sequence (423-450), which we postulated may be able to
295 bind in the LxVP binding pocket (Czirják & Enyedi, 2014). AlphaFold-Multimer was used
296 to predict the structure of the FAM126A-mediated interaction of PI4KA and Calcineurin
297 (Fig. 4B-C), with both sequences predicted to bind in the LxVP and PxIxIT binding sites
298 on Calcineurin, with predicted alignment error indicative of a stable interface.
299

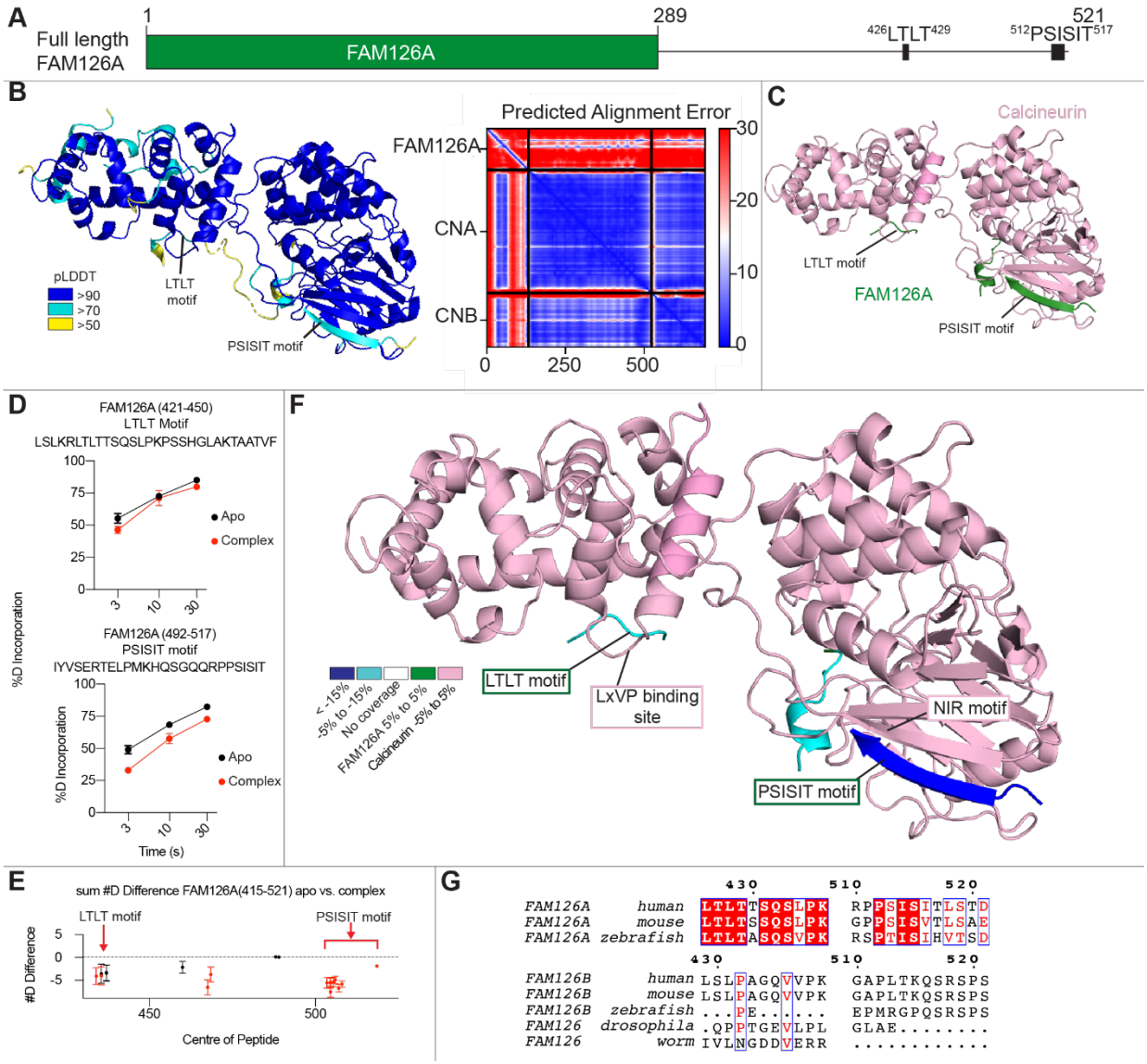

Figure 4. FAM126A LTLT motif interacts with CNB's LxVP binding site

A. Domain schematic of FAM126A highlighting the disordered C-terminal which contains conserved LTLT and PSISIT motifs.

B. (L) AlphaFold-Multimer model of Calcineurin in complex with the FAM126A C-terminal tail coloured with the per-residue confidence metric predicted local-distance difference test (pLDDT) as per the legend, and pLDDT <50 removed. (R) Predicted aligned error (PAE) of the AlphaFold-Multimer search of Calcineurin and the FAM126A C-terminal tail.

C. AlphaFold-Multimer model of Calcineurin in complex with the FAM126A C-terminal tail with pLDDT <60 removed. Domains are coloured according to the in-figure text.

310 **D.** Selected deuterium exchange time courses of FAM126A (415-521) and Calcineurin peptides that
311 showed significant (defined as >5% 0.45 Da, and p>0.01 in an unpaired two-tailed t test at any time point)
312 decreases in exchange. Error is shown as standard deviation (SD) (n=3).
313 **E.** Sum of the number of deuteron difference of FAM126A (415-521) upon complex formation with
314 Calcineurin analysed over the entire deuterium exchange time course for FAM126A (415-521). Each point
315 is representative of the centre residue of an individual peptide. Peptides that met the significance criteria
316 described in F are coloured red. Error is shown as the sum of standard deviations across all 3 time points
317 (SD) (n=3).
318 **F.** Peptides showing significant differences in deuterium exchange upon complex formation. Differences
319 are mapped on AlphaFold model shown in panel C. Differences are indicated by the legend.
320 **G.** Multiple sequence alignment of FAM126A (from *Homo sapiens, Mus musculus,* and *Danio rerio*) and
321 FAM126B/FAM126 (from *Homo sapiens, Mus musculus, Danio rerio, Drosophila melanogaster,* and
322 *Caenorhabditis elegans*.
323

324 **Discussion**

325 We had previously discovered that PI4KA was regulated by the plasma membrane
326 localised CNAβ1 isoform of Calcineurin, with Calcineurin playing a role in regulating PI4P
327 synthesis at the plasma membrane downstream of GPCR signaling (Ulengin-Talkish *et*
328 *al*, 2021). In this study we aimed to investigate the full complement of molecular
329 mechanisms underlying this regulatory role of Calcineurin in PI4KA signaling. Our
330 synergistic application of cryo-EM, HDX-MS, and AlphaFold modelling has established
331 that the PI4KA complex contains two proteins that have evolutionarily conserved and
332 distinct Calcineurin binding sites. PI4KA has two regions that bind Calcineurin, one
333 located in the horn domain, and one in the dimerization domain, with FAM126A binding
334 to Calcineurin through its disordered C-terminus.

335 An important question posed from this work, is the evolutionary mechanism
336 explaining why PI4KA has some of the largest variations in Calcineurin binding SLiM
337 motifs. This could be driven by CNAβ1 being the only Calcineurin isoform to be directly
338 localised to the plasma membrane through palmitoylation (Ulengin-Talkish *et al*, 2021),
339 with it being in high local concentration relative to PI4KA through its enrichment on
340 membrane surfaces. However, variation from the canonical LxVP and PxIxIT motifs in
341 Calcineurin regulated proteins has been observed, including Calcineurin binding proteins

342 containing IAIIIT (Li *et al*, 2012) and LVPP sequences at their binding sites (Li *et al*, 2020).
343 Another important unanswered question of our work is why the PI4KA complex has
344 evolved to have Calcineurin binding sites on both FAM126A and PI4KA. This is especially
345 puzzling as PI4KA can bind either FAM126A or FAM126B, with only FAM126A containing
346 a SLiM motif. Further cellular and organismal analysis of mutants in both the PI4KA and
347 FAM126A sites will be required to understand their precise role in PI4KA signaling, and
348 any FAM126A-specific functions in Calcineurin/PI4KA signaling.

349 Canonically, Calcineurin binds to substrate SLiM motifs to orient substrate
350 phosphorylation sites towards the active site of Calcineurin (Ulengin-Talkish & Cyert,
351 2023; Brauer *et al*, 2019; Wigington *et al*, 2020). We previously identified a CNAβ1
352 regulated phosphosite in the C-terminus of FAM126A (Ulengin-Talkish *et al*, 2021), which
353 suggested that there likely could be additional phosphorylation sites in the vicinity of the
354 PI4KA horn site. There is an annotated phosphorylation site at S1436 near the LVPP
355 motif in PI4KA, which could be dephosphorylated by Calcineurin. There are also
356 extensive phosphorylation sites present in the C-terminus of both TTC7A and TTC7B that
357 are in close spatial proximity to Calcineurin (Fig. S5A-C) (Hornbeck *et al*, 2015). These
358 sites are present in a disordered loop (642-703 in TTC7B, and 650-688 in TTC7A) that
359 would be accessible to the active site of Calcineurin when comparing AlphaFold models
360 of these loops to our cryo-EM structure (Fig. S5B-D). Intriguingly, this loop is in direct
361 proximity to the proposed binding site for EFR3, which recruits PI4KA to the plasma
362 membrane (Baskin *et al*, 2016). In yeast, phosphorylation of efr3 downregulates PI4KA
363 recruitment through decreased association with the TTC7 isoform Ypp1 (Wu *et al*, 2014).
364 Further experimentation defining the binding interface of EFR3 to the PI4KA complex
365 should consider the possible role of these PTMs in TTC7 in regulating PI4KA membrane
366 localisation and activity.

367 Overall, our work reveals important new insight into the molecular basis for how
368 CNAβ1 can bind to and regulate the PI4KA complex. The structural insight provided by
369 our work provides an exciting platform for continued investigations into how
370 phosphorylation regulates PI4KA, and how calcium signaling is integrated into PI4P
371 production at the plasma membrane.

Acknowledgements

JEB is supported by the Natural Science and Engineering Research council (Discovery grant NSERC-2020-04241), and a Michael Smith Foundation for Health Research (Scholar Award 17686). ALS was supported by an NSERC CGS-M scholarship. C.K.Y. is supported by CIHR (PJT-168907) and the Natural Sciences and Engineering Research Council of Canada (RGPIN-2018-03951). Cryo-EM specimens were prepared, and data was collected at the High Resolution Macromolecular Electron Microscopy (HRMEM) facility at the University of British Columbia (https://cryoem.med.ubc.ca). We thank Claire Atkinson, Joeseph Felt, Liam Worrall and Natalie Strynadka. HRMEM is funded by the Canadian Foundation for Innovation and the British Columbia Knowledge Development Fund.

Competing Interests

J.E.B. reports personal fees from Scorpion Therapeutics and Reactive therapeutics; and research contracts from Novartis and Calico Life Sciences.

Data Availability

The EM data have been deposited in the EM data bank with accession number (EMDB: 44382), and the associated structural model has been deposited to the PDB with accession number (PDB: 9B9G). The MS proteomics data have been deposited to the ProteomeXchange Consortium via the PRIDE (Perez-Riverol *et al*, 2022) partner repository with the dataset identifiers PXD043409 and PXD050633. All raw data in all figures are available in the source data excel file.

402 **Materials and Methods**

403

404 ***Multiple Sequence Alignments***

405 Multiple sequence alignments were generated using Clustal Omega. Aligned sequences
406 were then analysed by ESPript 3.0 (https://espript.ibcp.fr) (Gouet *et al*, 2003) to visualize
407 conservation. The uniprot accession codes for Figure 2C are P42356, E9Q3L2,
408 A0A8M3AWF4, Q9W4X4, Q9XW63, Q9USR3, and P37297. The uniprot accession
409 codes for Figure 2D are Q86TV6, Q9ULT0, E9Q6P5, Q8BGB2, A1L101, A0A8M9QA29,
410 A0A0B4K7H0, Q7KN74, H2KYB6, O94441, and P46951. The uniprot accession codes
411 for Figure 3G are P42356, E9Q3L2, Q49GP4, S4RUP9, ASA812BZT7, V4C7L9,
412 Q9W4X4, Q9XW63, Q9USR3, and P37297. The uniprot accession codes for Figure 4G
413 are Q9BYI3, Q6P9N1, Q6P121, Q8IXS8, Q8C729, A1A5W7, Q7K1C5, and Q6A586.

414

415 ***Protein Expression***

416 PI4KA complex (PI4KA/TTC7B full length, FAM126A (1-308)) was expressed from
417 bacmids harbouring MultiBac constructs which were transfected into *Spodoptera*
418 *frugiperda (Sf9) cells,* and viral stocks amplified for one generation to acquire a P2
419 generation viral stock. Final viral stocks were added to *Sf9 cells* in a 1/100 virus volume-
420 to-cell ratio. Constructs were expressed for 65-72 hours before pelleting of infected cells.
421 GST-tagged or SII-10xHis (2x strep with 10x his) human calcineurin A (aa 2-391 human
422 CNA alpha isoform) in tandem with calcineurin B were expressed in BL21 C41
423 *Escherichia coli*, induced with 0.1 mM IPTG (isopropyl β-d-1-thiogalactopyranoside) and
424 grown at 23°C overnight. SII-10xHis MBP tagged FAM126A (415-521) was expressed in
425 BL21 C41 *Escherichia coli* induced with 0.5 mM IPTG and grown at 37°C for 3 hours. Cell
426 pellets were washed with PBS immediately prior to being snap-frozen in liquid nitrogen,
427 then stored at -80°C.

428

429 ***Protein purification***

430 For PI4KA complex purification, *Sf9* pellets were re-suspended in lysis buffer [100 mM
431 NaCl, 20 mM imidazole (pH 8.0), 5% glycerol (v/v), 2 mM βMe, protease inhibitor

432 (Protease Inhibitor Cocktail Set III, EDTA-Free)] and lysed by sonication for 2.5 minutes.
433 Triton X-100 was added to a 0.1% (v/v) and centrifuged for 45 minutes at 20,000 g at 1°C
434 (Beckman Coulter J2-21, JA 20 rotor). The supernatant was loaded onto a 5 ml HisTrap
435 FF Crude column (Cytiva), washed with NiNTA A buffer [100mM NaCl, 20 mM imidazole
436 (pH 8.0), 5% glycerol (v/v), 2 mM βMe], washed with 10% NiNTA B buffer, and eluted
437 with NiNTA B buffer [100 mM NaCl, 450 mM imidazole (pH 8.0), 5% glycerol (v/v), 2 mM
438 βMe]. The eluent was loaded onto a 5 mL StrepTrap column (Cytiva) pre-equilibrated with
439 GFB [150 mM NaCl, 20 mM imidazole (pH 7.0), 5% glycerol (v/v), 0.5 mM TCEP] then
440 washed prior to the addition of a lipoyl domain containing TEV protease. TEV cleavage
441 proceeded overnight before elution with 10 mL of GFB. Protein was concentrated using
442 an Amicon 50 kDa MWCO concentrator (MilliporeSigma). PI4KA complex used for
443 crosslinking experiments with Calcineurin was taken after this concentration step (see
444 below, *Crosslinking*). PI4KA complex used for HDX-MS experiments was loaded onto a
445 pre-equilibrated [150 mM NaCl, 20 mM imidazole (pH 7.0), 5% glycerol (v/v), 0.5 mM
446 TCEP] Superose 6 Increase column (Cytiva) and protein-containing fractions were
447 collected, concentrated, flash frozen in liquid nitrogen, and stored at -80 °C.
448 *Escherichia coli* cell pellets containing GST-tagged human Calcineurin were lysed
449 by sonication for 5 minutes in lysis buffer [50 mM Tris (pH 8.0), 100 mM NaCl, 2 mM
450 EDTA, 2 mM EGTA, protease inhibitors (Millipore Protease Inhibitor Cocktail Set III,
451 Animal-Free)]. NaCl was then added to 1 M and the lysed solution was centrifuged at
452 20,000 g at 1°C for 45 minutes (Beckman Coulter J2-21, JA 20 rotor). Tween-20 was
453 added to the supernatant to 0.1% (v/v) then loaded onto a 5 mL GSTrap 4B column
454 (Cytiva) in a super loop fashion for 1 hour, then washed in Wash Buffer [50 mM Tris (pH
455 8.0), 110 mM KOAc, 2 mM MgOAc, 0.02% CHAPS (w/v), 5% glycerol (v/v) 0.5 mM TCEP]
456 to remove non-specifically bound protein. To remove GroEL chaperone the column was
457 washed with Wash buffer containing 2 mM ATP. To remove the GST tag, PreScission
458 protease was added to the column and incubated overnight at 4°C. The cleaved protein
459 was eluted with 7 mL of Wash Buffer. The eluant underwent size exclusion
460 chromatography (SEC) using a Superdex 200 10/300 column (Cytiva) equilibrated in GFB
461 [150 mM NaCl, 20 mM imidazole (pH 7.0), 5% glycerol (v/v), 0.5 mM TCEP] for

462 crosslinking experiments, or Wash Buffer [50 mM Tris (pH 8.0), 110 mM KOAc, 2 mM
463 MgOAc, 0.02% CHAPS (w/v), 5% glycerol (v/v) 0.5 mM TCEP]. For crosslinking reaction
464 (see below, *Crosslinking*), fresh, concentrated protein was used. In all other cases,
465 fraction(s) containing protein of interest were pooled, concentrated, flash frozen in liquid
466 nitrogen and stored at -80°C.

467 *Escherichia coli* cell pellets containing SII-10xHis tagged Calcineurin were lysed
468 by sonication for 5 minutes in lysis buffer (50 mM Tris pH 8.0 (RT), 100 mM NaCl, 2 mM
469 EDTA, 2 mM EGTA, 10 mM Imidazole pH 8.0 (RT), 2 mM βMe, protease inhibitors
470 (Millipore Protease Inhibitor Cocktail Set III, Animal-Free)). NaCl was added to 1 M and
471 the lysed solution was centrifuged at 20,000 g for 50 minutes at 4°C. Tween-20 was
472 added to the supernatant to 0.1% (v/v) then loaded onto a HisTrap FF Crude column
473 (Cytiva), washed with NiNTA A buffer [50 mM Tris pH 8.0 (RT), 100 mM NaCl, 2 mM
474 EDTA, 2 mM EGTA, 10 mM Imidazole pH 8.0 (RT),2 mM βMe], washed with 6% NiNTA
475 B buffer, and eluted with NiNTA B buffer [50 mM Tris pH 8.0 (RT), 100 mM NaCl, 2 mM
476 EDTA, 2 mM EGTA, 200 mM Imidazole pH 8.0 (RT),2 mM βMe]. The eluent was loaded
477 onto a 5 mL StrepTrap column pre-equilibrated with GFB [20 mM HEPES (pH 7.5) RT,
478 150 mM NaCl, 0.5 mM TCEP] then washed prior to the addition of a lipoyl domain
479 containing TEV protease. TEV cleavage proceeded overnight before elution with 12 mL
480 of GFB. The eluant underwent size exclusion chromatography (SEC) using a Superdex
481 200 10/300 column equilibrated in GFB [150 mM NaCl, 20 mM imidazole (pH 7.0), 5%
482 glycerol (v/v), 0.5 mM TCEP]. Fraction(s) containing protein of interest were pooled,
483 concentrated, flash frozen in liquid nitrogen and stored at -80°C

484 *Escherichia coli* cell pellets containing FAM126A (415-521) were lysed by
485 sonication for 5 minutes in lysis buffer (20 mM Tris pH 8.0 (RT), 100 mM NaCl, 20 mM
486 Imidazole pH 8.0 (RT), 5% Glycerol (v/v), 2 mM βMe, protease inhibitors (Millipore
487 Protease Inhibitor Cocktail Set III, Animal-Free)). The lysed solution underwent sonication
488 for 5 minutes prior to Triton-X being added to 0.1% (v/v). The solution was then
489 centrifuged at 20,000 g for 45 minutes at 2°C. The supernatant was then loaded onto a
490 HisTrap FF Crude column (Cytiva), washed with High Salt buffer buffer (20 mM Tris pH
491 8.0 (RT), 1 M NaCl, 20 mM Imidazole pH 8.0 (RT), 5% Glycerol (v/v), 2 mM βMe), NiNTA

492 A buffer (20 mM Tris pH 8.0 (RT), 100 mM NaCl, 20 mM Imidazole pH 8.0 (RT), 5%
493 Glycerol (v/v), 2 mM βMe), 6% NiNTA B, and eluted with NiNTA B (20 mM Tris pH 8.0
494 (RT), 100 mM NaCl, 250 mM Imidazole pH 8.0 (RT), 5% Glycerol (v/v), 2 mM βMe). The
495 eluent was loaded onto a 5 mL StrepTrap column pre-equilibrated in GFB (20 mM HEPES
496 pH 7.5 (RT), 150 mM NaCl, 5% Glycerol, 0.5 mM TCEP) and washed with GFB containing
497 0.5 M NaCl, an ATP wash (GFB with 2 mM ATP, 10 mM $MgCl_2$, and 150 mM KCl, a GFB
498 wash, and then eluted with GFB containing 2.5 mM desthiobiotin. Protein was
499 concentrated and injected onto a pre-equilibrated Superdex 200 10/300 column
500 equilibrated in GFB. Fractions containing protein were collected, aliquoted, flash frozen
501 in liquid nitrogen, and stored at -80°C.
502
503 ***PI4KA complex-Calcineurin size exclusion chromatography co-elution***
504 PI4KA complex (1.89 μM) and Calcineurin (8.17 μM) were incubated on ice for 15 minutes
505 prior to loading onto a Superose 6 Increase column pre-equilibrated in GFB [150 mM
506 NaCl, 20 mM imidazole (pH 7.0), 5% glycerol (v/v), 0.5 mM TCEP]. Fractions containing
507 the PI4KA complex bound to Calcineurin were pooled, concentrated, flash frozen in liquid
508 nitrogen and stored at -80°C. Fresh protein was run on an SDS-PAGE gel.
509
510 ***Electron Microscopy/Model Building***
511 *Protein sample preparation using BS^3 crosslinker:* PI4KA complex and Calcineurin were
512 incubated together on ice for 15 minutes at 2 μM and 4 μM, respectively. BS3 was added
513 to a final concentration of 1 mM and the reaction was incubated on ice for 2 hours. 1 M
514 Tris (pH 7.5) was added to 50 mM to quench the reaction and incubated at RT for 15
515 minutes. The quenched reaction was loaded onto Superose 6 Increase 10/300 column in
516 GFB [150 mM NaCl, 20 mM imidazole (pH 7.0), 5% glycerol (v/v), 0.5 mM TCEP].
517 Fractions encompassing the main peak, consistent with an elution volume of the complex,
518 were collected, concentrated, flash frozen in liquid nitrogen, and stored at -80°C.
519
520 *Cryo-EM sample preparation and data collection:* C-Flat 2/1-3Cu-T-50 grids were glow-
521 discharged for 25 s at 15 mA using a Pelco easiGlow glow discharger. 3 μl of PI4KA

522 complex crosslinked to Calcineurin were applied to the grids at 0.77 mg/ml and vitrified
523 using a Vitrobot Mark IV (FEI) by blotting for 1 second at a blot force of -5 at 4°C and
524 100% humidity. Specimens were screened using a 200-kV Glacios transmission
525 microscope (Thermo Fisher Scientific) equipped with a Falcon 3EC direct electron
526 detector (DED). Datasets were collected using a 300-kV Titan Krios equipped with a
527 Falcon 4i camera and the Selectris energy filter. A total of 10,121 super-resolution movies
528 were collected using SerialEM with a total dose of 50 $e^-/Å^2$ over 603 frames at a physical
529 pixel size of 0.77 Å per pixel, using a defocus range of -1 to -2 um, at 165,000 x
530 magnification.
531
532 *Cryo-EM image processing:* All data processing was carried out using cryoSPARC v4.2.1.
533 Patch motion correction using default settings was applied to all movies to align the
534 frames and Fourier-crop the outputs by a factor of 2. The contrast transfer function (CTF)
535 of the resulting micrographs was estimated using the patch CTF estimation job with
536 default settings. Micrographs were manually curated to contain only micrographs with
537 CTF fit resolution less than or equal to 10.
538 To generate an initial model, 222,684 particles were picked from 2784 micrographs
539 using blob picking with a minimum and maximum diameter of 250 and 280, respectively.
540 Particles were inspected using the inspect picks job to remove particles that picked ice
541 contamination and were then extracted with a box size of 480 pixels and a Fourier
542 cropping of the output by a factor of 4, for a total of 154,266 particles. The particles were
543 subjected to two rounds of 2D classification. A total of 43,673 particles were used for *ab*
544 *initio* reconstruction and heterogeneous refinement using two classes, with C1 symmetry.
545 The best heterogeneous refinement then underwent one round of homogeneous
546 refinement with C1 symmetry. This was used to create 2D templates using cryoSPARC's
547 create templates job, which were used to pick particles from the complete dataset.
548 To generate a cryo-EM map from the complete dataset, the above 2D templates
549 were low pass filtered to 20 Å and used to template pick 9,830 micrographs with the
550 particle diameter set to 450 Å. 1,181,312 particles were inspected and 604,191 were
551 extracted with a box size of 1200 pixels and the outputs were Fourier-cropped by a factor

552 of 2.08, and subjected to 2D classification with 40 online-EM iterations to remove particles
553 with ice contamination or those who showed no features. 428,725 particles were used for
554 *ab initio* reconstruction and heterogeneous refinement using two classes and C1
555 symmetry. 239,931 particles from the best reconstruction underwent local motion
556 correction and a subsequent *ab initio* reconstruction and heterogeneous refinement with
557 two classes. A total of 235,760 particles were used to carry out a homogeneous
558 refinement with C1 symmetry using the previous 3D reconstruction as the starting model,
559 yielding a reconstruction with an overall resolution of 3.51 Å based on the Fourier shell
560 correlation (FSC) 0.143 criterion. The full workflow to generate the final cryo-EM map is
561 shown in Extended Figure 1.
562
563 *AlphaFold:* We used the protein prediction software, AlphaFold to predict where
564 Calcineurin interacts with PI4KA. Specifically, AlphaFold2 using Mmseqs2 Google Colab
565 (https://colab.research.google.com/github/sokrypton/ColabFold/blob/main/AlphaFold2.ip
566 ynb) was used to model the structure of the PI4KA horn (aa 1-1100), the horn-dimerization
567 domains of PI4KA (aa 400-1500) or FAM126A (aa 390-521) in complex with Calcineurin
568 (CNA alpha: aa 2-391, and CNB) without templates (Mirdita *et al*, 2022; Jumper *et al*,
569 2021). AlphaFold generated five models ranked in order by mean pLDDT. The predicted
570 aligned error (PAE) for the top-ranked outputs are shown in Figure 3B and 4B.
571
572 *Model building:* The cryo EM structure of PI4KA-TTC7B-FAM126A (PDB: 6BQ1) (Lees *et*
573 *al*, 2017) was fit into the map using Chimera (Pettersen *et al*, 2004). The horn domain of
574 PI4KA was at higher local resolution than the original data, and allowed for iterative
575 rounds of automated model building in Phenix guided by secondary structure predicted
576 by AlphaFold modelling (Jumper *et al*, 2021), manual model building in COOT, and
577 refinement in Phenix.real_space_refine using realspace, rigid body, and adp refinement
578 with tight secondary structure restraints (Afonine *et al*, 2012). This allowed for building
579 the full solenoid horn domain with high confidence.
580 The local resolution of Calcineurin was the lowest of any protein chains, although
581 the high resolution structure of Calcineurin (PDB: 6NUC) (Hendus-Altenburger *et al*,

582 2019) could be fit into the density. We then used the AlphaFold-Multimer search result for
583 Calcineurin bound to the beta strand of PI4KA (see previous section), and fit into the map
584 using Chimera (Pettersen *et al*, 2004). The entire model was refined using
585 Phenix.real_space_refine using rigid body, adp refinement with both reference model
586 restraints using the high resolution Calcineurin model 6NUC and tight secondary structure
587 restraints (Afonine *et al*, 2012). The full refinement and validation statistics are shown in
588 Supplementary Table 1.
589
590 ***HDX-MS***
591 *HDX-MS sample preparation:* Initial HDX reactions comparing PI4KA complex apo and
592 Calcineurin apo to PI4KA complex + Calcineurin were carried out in an 8.16 μl reaction
593 volume containing 11 pmol of both proteins. The exchange reactions were initiated by the
594 addition of 5.88 μL of D_2O buffer (20 mM Imidazole pH 7, 150 mM NaCl, 93.9% D_2O (V/V))
595 to 2.88 μL of protein (final D_2O concentration of 67.7%). Reactions proceeded for 3s, 30s,
596 and 300s at room temperature (18°C) before being quenched with ice cold acidic quench
597 buffer, resulting in a final concentration of 0.6M guanidine HCl and 0.9% formic acid post
598 quench. HDX reactions comparing PI4KA complex apo to PI4KA complex + Calcineurin
599 were then carried out at pH 6.5 to capture changes in disordered and flexible regions of
600 the PI4KA complex. Reactions occurred in an 8.12 μl reaction volume containing 10 pmol
601 of PI4KA complex and 20 pmol of Calcineurin. The exchange reactions were initiated by
602 the addition of 5.74 μL of D_2O buffer (20 mM MES pH 6.5, 150 mM NaCl, 1 mM $CaCl_2$,
603 93.37% D_2O (V/V)) to 2.38 μL of protein (final D_2O concentration of 67%). Reactions
604 proceeded for 3s, 10s, and 30s at 0°C before being quenched with ice cold acidic quench
605 buffer, resulting in a final concentration of 0.6M guanidine HCl and 0.9% formic acid post
606 quench. All conditions and time points were created and run in independent triplicate.
607 Samples were flash frozen immediately after quenching and stored at -80°C.
608 HDX reactions comparing FAM126A (415-521) apo to FAM126A (415-521) +
609 Calcineurin were carried out in a 12 μl reaction volume containing 30 pmol of both
610 proteins. The exchange reactions were initiated by the addition of 9 μL of D_2O buffer (20
611 mM MES pH 6.5, 150 mM NaCl, 1mM $CaCl_2$, 93.4% D_2O (V/V)) to 3 μL of protein (final

612 D_2O concentration of 70%). Reactions proceeded for 3s, 10s, and 30s at 0°C, pH 6.5
613 before being quenched with ice cold acidic quench buffer, resulting in a final concentration
614 of 0.6M guanidine HCl and 0.9% formic acid post quench. All conditions and time points
615 were created and run in independent triplicate. A fully deuterated sample was made by
616 incubating 1 μl of 30 μM FAM126A (415-521) with 7 M guanidine HCl (final 4.67M), heated
617 to 90°C for five minutes followed by two minutes 20°C, followed by the addition of 9 μl of
618 D_2O buffer (20 mM MES pH 6.5, 150 mM NaCl, 1 mM $CaCl_2$, 93.37% D_2O (V/V)) for 10
619 minutes at 50°C then two minutes at 20°C for 2 minutes, and then 0°C for 2 minutes
620 before being quenched as above. Samples were flash frozen immediately after quenching
621 and stored at -80°C.
622
623 *Protein digestion and MS/MS data collection:* Protein samples were rapidly thawed and
624 injected onto an integrated fluidics system containing a HDx-3 PAL liquid handling robot
625 and climate-controlled (2°C) chromatography system (Trajan), a Dionex Ultimate 3000
626 UHPLC system (Thermofisher), or a Acquity UPLC I-Class Series System (Waters), as
627 well as an Impact HD QTOF Mass spectrometer (Bruker). The full details of the automated
628 LC system are described in (Stariha *et al*, 2021). Samples comparing PI4KA complex apo
629 and Calcineurin apo to PI4KA complex + Calcineurin (pH 7.0, 18°C) were run over one
630 immobilized pepsin column (Trajan; ProDx protease column, 2.1 mm x 30 mm,
631 PDX.PP01-F32) at 200 μL/min for 3 minutes at 10°C. Samples comparing FAM126A
632 (415-521) apo to FAM126A (415-521) + Calcineurin and samples comparing PI4KA
633 complex apo to PI4KA complex + Calcineurin (pH 6.5, 0°C) were run over an immobilized
634 pepsin column (Affipro; AP-PC-001) at 200 μL/min for 4 minutes at 2°C. The resulting
635 peptides were collected and desalted on a C18 trap column (ACQUITY UPLC BEH C18
636 1.7 μm column, 2.1 mm x 5 mm; Waters 186004629). The trap was subsequently eluted
637 in line with an ACQUITY 1.7 μm particle, 2.1 mm × 100 mm C18 UPLC column (Waters;
638 186003686), using a gradient of 3-35% B (Buffer A 0.1% formic acid; Buffer B 100%
639 acetonitrile) over 11 minutes immediately followed by a gradient of 35-80% over 5
640 minutes. Mass spectrometry experiments were acquired over a mass range from 150 to

641 2200 m/z using an electrospray ionization source operated at a temperature of 200°C and
642 a spray voltage of 4.5 kV.
643
644 *Peptide identification:* Peptides were identified from the non-deuterated samples of the
645 PI4KA complex, Calcineurin, or FAM126A (415-521) using data-dependent acquisition
646 following tandem MS/MS experiments (0.5 s precursor scan from 150-2000 m/z; twelve
647 0.25 s fragment scans from 150-2000 m/z). For HDX reactions comparing PI4KA complex
648 apo and Calcineurin apo to PI4KA complex + Calcineurin (pH 7.0, 18°C), MS/MS datasets
649 were analysed using PEAKS7 (PEAKS), and peptide identification was carried out by
650 using a false discovery based approach, with a threshold set to 0.1% using a database
651 of purified proteins and known contaminants (Dobbs *et al*, 2020a). The search parameters
652 were set with a precursor tolerance of 20 ppm, fragment mass error 0.02 Da, charge
653 states from 1-8, with a -10logP score of 31.9 and 15 for the PI4KA complex or Calcineurin
654 respectively. For HDX reactions comparing PI4KA complex apo to PI4KA complex +
655 Calcineurin at pH 6.5, and FAM126A (415-521) apo to FAM126A (415-521) in complex
656 with Calcineurin, MS/MS datasets were analysed using FragPipe v18.0 and peptide
657 identification was carried out by using a false discovery-based approach using a database
658 of purified proteins and known contaminants (Kong *et al*, 2017; da Veiga Leprevost *et al*,
659 2020; Dobbs *et al*, 2020b). MSFragger was utilised, and the precursor mass tolerance
660 error was set to -20 to 20 ppm. The fragment mass tolerance was set at 20 ppm. Protein
661 digestion was set as nonspecific, searching between lengths of 4 and 50 aa, with a mass
662 range of 400 to 5000 Da.
663
664 *Mass Analysis of Peptide Centroids and Measurement of Deuterium Incorporation:* HD-
665 Examiner Software (Sierra Analytics) was used to automatically calculate the level of
666 deuterium incorporation into each peptide. All peptides were manually inspected for
667 correct charge state, correct retention time, appropriate selection of isotopic distribution,
668 etc. Deuteration levels were calculated using the centroid of the experimental isotope
669 clusters. Results are presented as relative levels of deuterium incorporation and the only
670 control for back exchange in the PI4KA complex containing experiments was the level of

671 deuterium present in the buffer (67.7% and 67%). For FAM126A (415-521) HDX
672 experiments, back exchange was controlled for by generating a fully deuterated sample.
673 For all HDX-MS experiments, differences in exchange in a peptide were considered
674 significant if they met all three of the following criteria: ≥5% change in exchange, ≥0.45
675 Da difference in exchange, and a p value <0.01 using a two tailed student t-test. The raw
676 HDX data are shown in two different formats. The raw peptide deuterium incorporation
677 graphs for a selection of peptides with significant differences are shown in Figures
678 3C/4D/S4B-E/S4G, with the raw data for all analysed peptides in the source data. To
679 allow for visualization of differences across all peptides, we utilised number of deuteron
680 difference (#D) plots (Fig. 3E/4E/S4A/S4F). These plots show the total difference in
681 deuterium incorporation over the entire H/D exchange time course, with each point
682 indicating a single peptide. Samples were only compared within a single experiment and
683 were never compared to experiments completed at a different time with a different final
684 D_2O level. The data analysis statistics for all HDX-MS experiments are in the source data
685 file according to the guidelines of (Masson *et al*, 2019). The mass spectrometry
686 proteomics data have been deposited to the ProteomeXchange Consortium via the
687 PRIDE partner repository (Perez-Riverol *et al*, 2022) with the dataset identifiers
688 PXD043409 and PXD050633.
689
690 **References**

691 Afonine PV, Grosse-Kunstleve RW, Echols N, Headd JJ, Moriarty NW, Mustyakimov M,
692 Terwilliger TC, Urzhumtsev A, Zwart PH & Adams PD (2012) Towards
693 automated crystallographic structure refinement with phenix.refine. *Acta*
694 *Crystallogr D Biol Crystallogr* 68: 352–367
695 Baek M, DiMaio F, Anishchenko I, Dauparas J, Ovchinnikov S, Lee GR, Wang J, Cong
696 Q, Kinch LN, Schaeffer RD, *et al* (2021) Accurate prediction of protein structures
697 and interactions using a three-track neural network. *Science* 373: 871–876
698 Baird D, Stefan C, Audhya A, Weys S & Emr SD (2008) Assembly of the PtdIns 4-
699 kinase Stt4 complex at the plasma membrane requires Ypp1 and Efr3. *J Cell Biol*
700 183: 1061–1074
701 Balla T (2013) Phosphoinositides: tiny lipids with giant impact on cell regulation. *Physiol*
702 *Rev* 93: 1019–1137
703 Barlow-Busch I, Shaw AL & Burke JE (2023) PI4KA and PIKfyve: Essential
704 phosphoinositide signaling enzymes involved in myriad human diseases. *Curr*
705 *Opin Cell Biol* 83: 102207

Baskin JM, Wu X, Christiano R, Oh MS, Schauder CM, Gazzerro E, Messa M, Baldassari S, Assereto S, Biancheri R, *et al* (2016) The leukodystrophy protein FAM126A (hyccin) regulates PtdIns(4)P synthesis at the plasma membrane. *Nat Cell Biol* 18: 132–138

Batrouni AG & Baskin JM (2021) The chemistry and biology of phosphatidylinositol 4-phosphate at the plasma membrane. *Bioorg Med Chem* 40: 116190

Bigorgne AE, Farin HF, Lemoine R, Mahlaoui N, Lambert N, Gil M, Schulz A, Philippet P, Schlesser P, Abrahamsen TG, *et al* (2014) TTC7A mutations disrupt intestinal epithelial apicobasal polarity. *J Clin Invest* 124: 328–337

Boura E & Nencka R (2015) Phosphatidylinositol 4-kinases: Function, structure, and inhibition. *Exp Cell Res*

Brauer BL, Moon TM, Sheftic SR, Nasa I, Page R, Peti W & Kettenbach AN (2019) Leveraging New Definitions of the LxVP SLiM To Discover Novel Calcineurin Regulators and Substrates. *ACS Chem Biol* 14: 2672–2682

Burke JE, Triscott J, Emerling BM & Hammond GRV (2023) Beyond PI3Ks: targeting phosphoinositide kinases in disease. *Nat Rev Drug Discov* 22: 357–386

Chung J, Torta F, Masai K, Lucast L, Czapla H, Tanner LB, Narayanaswamy P, Wenk MR, Nakatsu F & De Camilli P (2015) INTRACELLULAR TRANSPORT. PI4P/phosphatidylserine countertransport at ORP5- and ORP8-mediated ER-plasma membrane contacts. *Science* 349: 428–432

Coales SJ, E SY, Lee JE, Ma A, Morrow JA & Hamuro Y (2010) Expansion of time window for mass spectrometric measurement of amide hydrogen/deuterium exchange reactions. *Rapid Commun Mass Spectrom* 24: 3585–3592

Czirják G & Enyedi P (2014) The LQLP calcineurin docking site is a major determinant of the calcium-dependent activation of human TRESK background K+ channel. *J Biol Chem* 289: 29506–29518

Dobbs JM, Jenkins ML & Burke JE (2020a) Escherichia coli and Sf9 Contaminant Databases to Increase Efficiency of Tandem Mass Spectrometry Peptide Identification in Structural Mass Spectrometry Experiments. *J Am Soc Mass Spectrom* 31: 2202–2209

Dobbs JM, Jenkins ML & Burke JE (2020b) Escherichia coli and Sf9 Contaminant Databases to Increase Efficiency of Tandem Mass Spectrometry Peptide Identification in Structural Mass Spectrometry Experiments. *J Am Soc Mass Spectrom* 31: 2202–2209

Dornan GL, Dalwadi U, Hamelin DJ, Hoffmann RM, Yip CK & Burke JE (2018) Probing the Architecture, Dynamics, and Inhibition of the PI4KIIIα/TTC7/FAM126 Complex. *J Mol Biol* 430: 3129–3142

Dornan GL, McPhail JA & Burke JE (2016) Type III phosphatidylinositol 4 kinases: structure, function, regulation, signalling and involvement in disease. *Biochemical Society Transactions* 44: 260–266

Gouet P, Robert X & Courcelle E (2003) ESPript/ENDscript: Extracting and rendering sequence and 3D information from atomic structures of proteins. *Nucleic Acids Res* 31: 3320–3323

749 Hammond GRV & Burke JE (2020) Novel roles of phosphoinositides in signaling, lipid
750 transport, and disease. *Curr Opin Cell Biol* 63: 57–67
751 Hendus-Altenburger R, Wang X, Sjøgaard-Frich LM, Pedraz-Cuesta E, Sheftic SR,
752 Bendsøe AH, Page R, Kragelund BB, Pedersen SF & Peti W (2019) Molecular
753 basis for the binding and selective dephosphorylation of Na+/H+ exchanger 1 by
754 calcineurin. *Nat Commun* 10: 3489
755 Hornbeck PV, Zhang B, Murray B, Kornhauser JM, Latham V & Skrzypek E (2015)
756 PhosphoSitePlus, 2014: mutations, PTMs and recalibrations. *Nucleic Acids Res*
757 43: D512-20
758 Jumper J, Evans R, Pritzel A, Green T, Figurnov M, Ronneberger O, Tunyasuvunakool
759 K, Bates R, Žídek A, Potapenko A, *et al* (2021) Highly accurate protein structure
760 prediction with AlphaFold. *Nature* 596: 583–589
761 Kong AT, Leprevost FV, Avtonomov DM, Mellacheruvu D & Nesvizhskii AI (2017)
762 MSFragger: ultrafast and comprehensive peptide identification in mass
763 spectrometry-based proteomics. *Nat Methods* 14: 513–520
764 Lees JA, Zhang Y, Oh MS, Schauder CM, Yu X, Baskin JM, Dobbs K, Notarangelo LD,
765 De Camilli P, Walz T, *et al* (2017) Architecture of the human PI4KIIIα lipid kinase
766 complex. *Proc Natl Acad Sci U S A* 114: 13720–13725
767 Li H, Pink MD, Murphy JG, Stein A, Dell'Acqua ML & Hogan PG (2012) Balanced
768 interactions of calcineurin with AKAP79 regulate Ca2+-calcineurin-NFAT
769 signaling. *Nat Struct Mol Biol* 19: 337–345
770 Li Y, Sheftic SR, Grigoriu S, Schwieters CD, Page R & Peti W (2020) The structure of
771 the RCAN1:CN complex explains the inhibition of and substrate recruitment by
772 calcineurin. *Sci Adv* 6: eaba3681
773 Masson GR, Burke JE, Ahn NG, Anand GS, Borchers C, Brier S, Bou-Assaf GM, Engen
774 JR, Englander SW, Faber J, *et al* (2019) Recommendations for performing,
775 interpreting and reporting hydrogen deuterium exchange mass spectrometry
776 (HDX-MS) experiments. *Nat Methods* 16: 595–602
777 Masson GR, Jenkins ML & Burke JE (2017) An overview of hydrogen deuterium
778 exchange mass spectrometry (HDX-MS) in drug discovery. *Expert Opin Drug*
779 *Discov* 12: 981–994
780 Mirdita M, Schütze K, Moriwaki Y, Heo L, Ovchinnikov S & Steinegger M (2022)
781 ColabFold: making protein folding accessible to all. *Nat Methods* 19: 679–682
782 Nakatsu F, Baskin JM, Chung J, Tanner LB, Shui G, Lee SY, Pirruccello M, Hao M,
783 Ingolia NT, Wenk MR, *et al* (2012) PtdIns4P synthesis by PI4KIIIα at the plasma
784 membrane and its impact on plasma membrane identity. *J Cell Biol* 199: 1003–
785 1016
786 Parson MAH, Jenkins ML & Burke JE (2022) Investigating how intrinsically disordered
787 regions contribute to protein function using HDX-MS. *Biochem Soc Trans* 50:
788 1607–1617
789 Pemberton JG, Kim YJ, Humpolickova J, Eisenreichova A, Sengupta N, Toth DJ, Boura
790 E & Balla T (2020) Defining the subcellular distribution and metabolic channeling
791 of phosphatidylinositol. *J Cell Biol* 219: e201906130

Perez-Riverol Y, Bai J, Bandla C, García-Seisdedos D, Hewapathirana S, Kamatchinathan S, Kundu DJ, Prakash A, Frericks-Zipper A, Eisenacher M, *et al* (2022) The PRIDE database resources in 2022: a hub for mass spectrometry-based proteomics evidences. *Nucleic Acids Res* 50: D543–D552

Pettersen EF, Goddard TD, Huang CC, Couch GS, Greenblatt DM, Meng EC & Ferrin TE (2004) UCSF Chimera--a visualization system for exploratory research and analysis. *J Comput Chem* 25: 1605–1612

Salter CG, Cai Y, Lo B, Helman G, Taylor H, McCartney A, Leslie JS, Accogli A, Zara F, Traverso M, *et al* (2021) Biallelic PI4KA variants cause neurological, intestinal and immunological disease. *Brain* 144: 3597–3610

Stariha JTB, Hoffmann RM, Hamelin DJ & Burke JE (2021) Probing Protein–Membrane Interactions and Dynamics Using Hydrogen–Deuterium Exchange Mass Spectrometry (HDX-MS). In *Protein-Ligand Interactions: Methods and Applications*, Daviter T Johnson CM McLaughlin SH & Williams MA (eds) pp 465–485. New York, NY: Springer US

Suresh S & Burke JE (2023) Structural basis for the conserved roles of PI4KA and its regulatory partners and their misregulation in disease. *Adv Biol Regul* 90: 100996

Ulengin-Talkish I & Cyert MS (2023) A cellular atlas of calcineurin signaling. *Biochim Biophys Acta Mol Cell Res* 1870: 119366

Ulengin-Talkish I, Parson MAH, Jenkins ML, Roy J, Shih AZL, St-Denis N, Gulyas G, Balla T, Gingras A-C, Várnai P, *et al* (2021) Palmitoylation targets the calcineurin phosphatase to the phosphatidylinositol 4-kinase complex at the plasma membrane. *Nat Commun* 12: 6064

da Veiga Leprevost F, Haynes SE, Avtonomov DM, Chang H-Y, Shanmugam AK, Mellacheruvu D, Kong AT & Nesvizhskii AI (2020) Philosopher: a versatile toolkit for shotgun proteomics data analysis. *Nat Methods* 17: 869–870

Verdura E, Rodríguez-Palmero A, Vélez-Santamaria V, Planas-Serra L, de la Calle I, Raspall-Chaure M, Roubertie A, Benkirane M, Saettini F, Pavinato L, *et al* (2021) Biallelic PI4KA variants cause a novel neurodevelopmental syndrome with hypomyelinating leukodystrophy. *Brain* 144: 2659–2669

Wigington CP, Roy J, Damle NP, Yadav VK, Blikstad C, Resch E, Wong CJ, Mackay DR, Wang JT, Krystkowiak I, *et al* (2020) Systematic Discovery of Short Linear Motifs Decodes Calcineurin Phosphatase Signaling. *Mol Cell* 79: 342-358.e12

Wu X, Chi RJ, Baskin JM, Lucast L, Burd CG, De Camilli P & Reinisch KM (2014) Structural insights into assembly and regulation of the plasma membrane phosphatidylinositol 4-kinase complex. *Developmental Cell* 28: 19–29

Zara F, Biancheri R, Bruno C, Bordo L, Assereto S, Gazzerro E, Sotgia F, Wang XB, Gianotti S, Stringara S, *et al* (2006) Deficiency of hyccin, a newly identified membrane protein, causes hypomyelination and congenital cataract. *Nat Genet* 38: 1111–1113

Zewe JP, Miller AM, Sangappa S, Wills RC, Goulden BD & Hammond GRV (2020) Probing the subcellular distribution of phosphatidylinositol reveals a surprising lack at the plasma membrane. *J Cell Biol* 219: e201906127

836 **Supplemental Figures Tables**

837 **Table S1 Cryo-EM data collection, refinement, and validation statistics**

	PI4KA/TTC7B/FAM126A (1-308)/Calcineurin EMD- 44382 PDB:9B9G
Data collection and processing	
Magnification	165,000
Voltage (kV)	300
Electron exposure (e/ Å^2)	50
Defocus range (μM)	1.0-2.0
Pixel size (Å)	0.77
Symmetry imposed	C1
Initial particle images (no.)	604,191
Final particle images (no.)	235,760
Map resolution (Å)	3.51
FSC threshold	0.143
Map resolution range (Å)	3.3-10
Refinement	
Initial model used (PDB)	6BQ1,6NUC
Model Resolution (Å)	3.51
FSC threshold	0.143
Map sharpening B factor	
Model composition	
Non-hydrogen atoms	51,176
Protein residues	6393
Ligands	8
B-factors	
Protein	186.5
Validation	
Mol probability score	2.01
Clashscore	12.44
Poor rotamers (%)	0.80
Ramachandran	
Favored	93.91
Allowed	6.09
Outliers	0.0
R.m.s. deviations	
Bond lengths (Å)	0.004
Bond angles (°)	0.809

838
839
840
841
842

843 **Table S2 Key Reagent/Resources**

REAGENT or RESOURCE	SOURCE	IDENTIFIER
Bacterial and virus strains		
E.coli DH10EMBacY Competent Cells	Geneva Biotech	DH10EMBacY
E.coli C41(DE3) chemically competent cells	Lab stock	
Chemicals, peptides, and recombinant proteins		
Deuterium Oxide 99.9%	Sigma Aldrich	151882-10X1ML
BS^3	Thermo Scientific	21580
Deposited Data		
Mass spectrometry proteomics data	This paper	PXD043409 PXD050633
PDB	This paper	9B9G
EMDB	This paper	44382
Recombinant DNA		
PI4KA complex PI4KA/TTC7B/FAM126A (1-308)	Dornan et al., 2018	GD177
Calcineurin-GST expression vector	Ulengen-Talkish et al., 2021	Calcineurin
Calcineurin strep-his expression vector	This paper	AS27
MBP-FAM126A (415-521)	This paper	AS39
Software and algorithms		
cryoSPARC v4.2.1	Structura Bio	https://cryosparc.com
Phenix-1.19.1	Open source	https://phenix-online.org/
COOT-0.9.4.1	CCP4	https://www2.mrc-lmb.cam.ac.uk/personal/pemsley/coot/
HDExaminer	Sierra Analytics	http://massspec.com/hdexaminer
Bruker Compass DataAnalysis 4.2	Bruker	www.bruker.com
GraphPad Prism 7	GraphPad	https://www.graphpad.com
PEAKS 7	Bioinformatics Solutions Inc.	https://www.bioinfor.com/versions/
FragPipe (v19.1)	Nesvizhskii Lab- University of Michigan	fragpipe.nesvilab.org
Adobe Illustrator	Adobe	https://www.adobe.com/products/illustrator.html
ESPript 3.0	SBGrid consortium	https:espript.ibcp.fr
PyMOL	Schroedinger	http://pymol.org
Other		
C-flat Holey Thick Carbon Grid 2.0 μm hole 1.0 μm space 300 mesh	Electron Microscopy Studies	CFT312-100

SF9 insect cells for expression	Expression Systems	94-001S
Affipro pepsin column, 69.3 μL, 2.1 mm X 20 mm	Affipro	AP-PC-001
ProDx Pepsin Column F 10-32	Trajan Scientific Americas	PDX.PP01-F32
ACQUITY UPLC Peptide BEH C18 Column, 300Å, 1.7 μm, 2.1 mm X 100 mm, 1K – 30K	Waters	186003686
ACQUITY UPLC BEH C18 1.7 μm, 2.1 mm x 5 mm	Waters	186004629

844
845

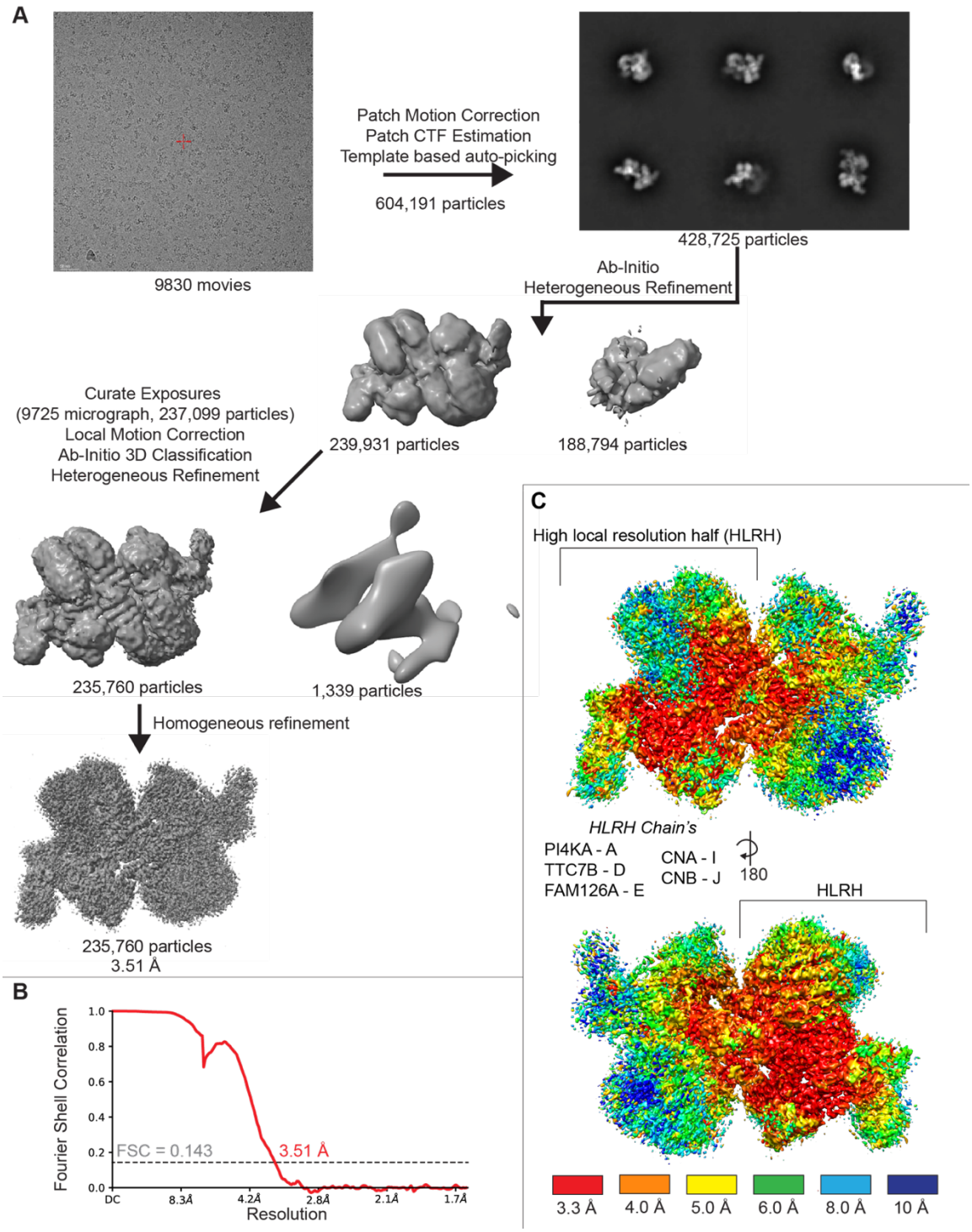

Supplemental Figure 1. Cryo-EM data processing

A. Cryo-EM data processing workflow showing a representative micrograph from screening on the 200 kV Glacios, representative 2D class averages, and the image processing strategy used to generate a 3D reconstruction of the PI4KA/TTC7B/FAM126A/Calcineurin complex.

B. Gold standard Fourier shell correlation coefficient (FSC) curve after auto tightening by cryoSPARC for the final PI4KA/TTC7B/FAM126A/ Calcineurin map.

C. Final PI4KA/TTC7B/FAM126A/ Calcineurin map coloured according to local resolution estimated using cryoSPARC v4.2.1

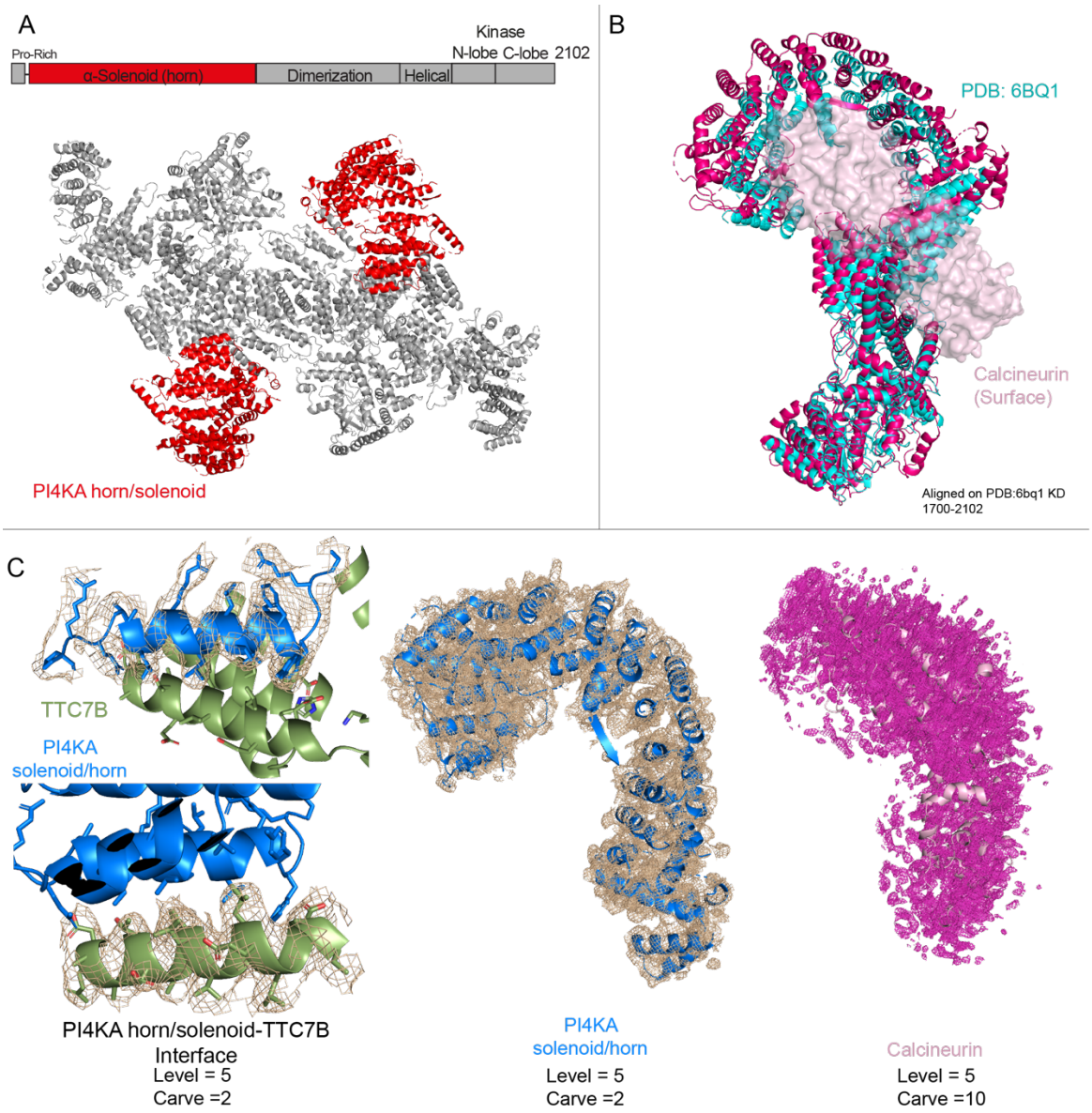

Supplemental Figure 2. Model density fit

A. Unique features in the PI4KA complex resolved from the cryo-EM map of the PI4KA complex interacting with Calcineurin. Red areas represent unique features, annotated on the domain schematic, and mapped onto the structural model with Calcineurin removed.

B. Comparison of the PI4KA structure from our study (magenta) to PI4KA from PI4KA/TTC7B/FAM126A (2-289) (cyan) apo (PDB:6BQ1) (Lees *et al*, 2017). Our model was aligned to 6BQ1 using residues 1700-2102.

C. Electron density of selected regions. (L) TTC7B-PI4KA solenoid/horn interface, with density for the N-terminal helix of PI4KA shown on top, and the density for the TTC7B interface helix shown on bottom (M) PI4KA solenoid/horn (aa 27-931), and (R) Calcineurin.

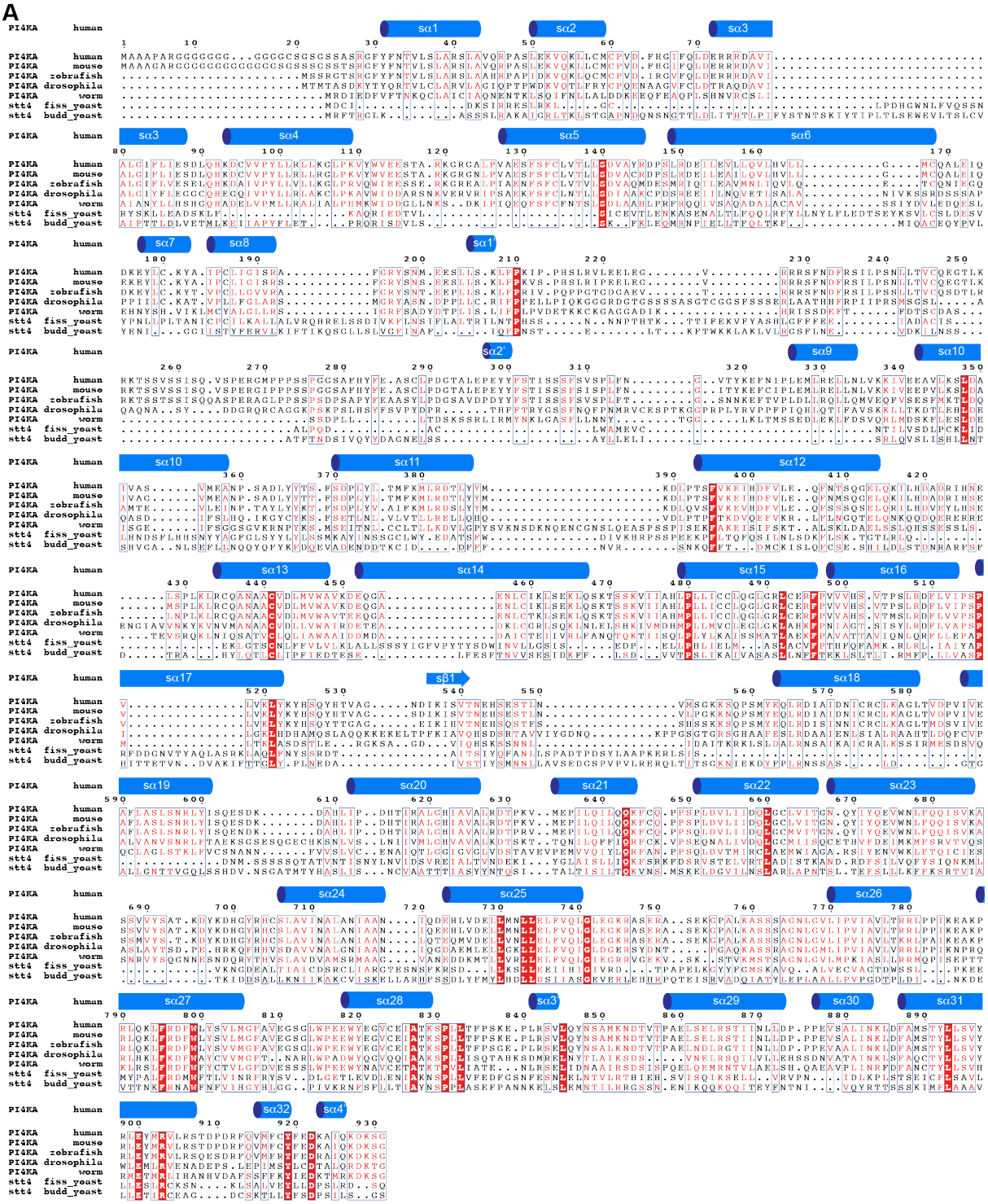

Supplemental Figure 3. Secondary structure annotation of PI4KA solenoid/horn

A. Multiple sequence alignment (generated with ESPript 3.0) of PI4KA from *Homo sapiens, Mus musculus, Danio rerio, Drosophila melanogaster, Caenorhabditis elegans*, *Schizosaccharomyces pombe,* and *Saccharomyces cerevisiae.* Secondary structure elements from the human PI4KA horn region, as determined from the cryo-EM map of the PI4KA complex bound to Calcineurin, are illustrated above the alignment.

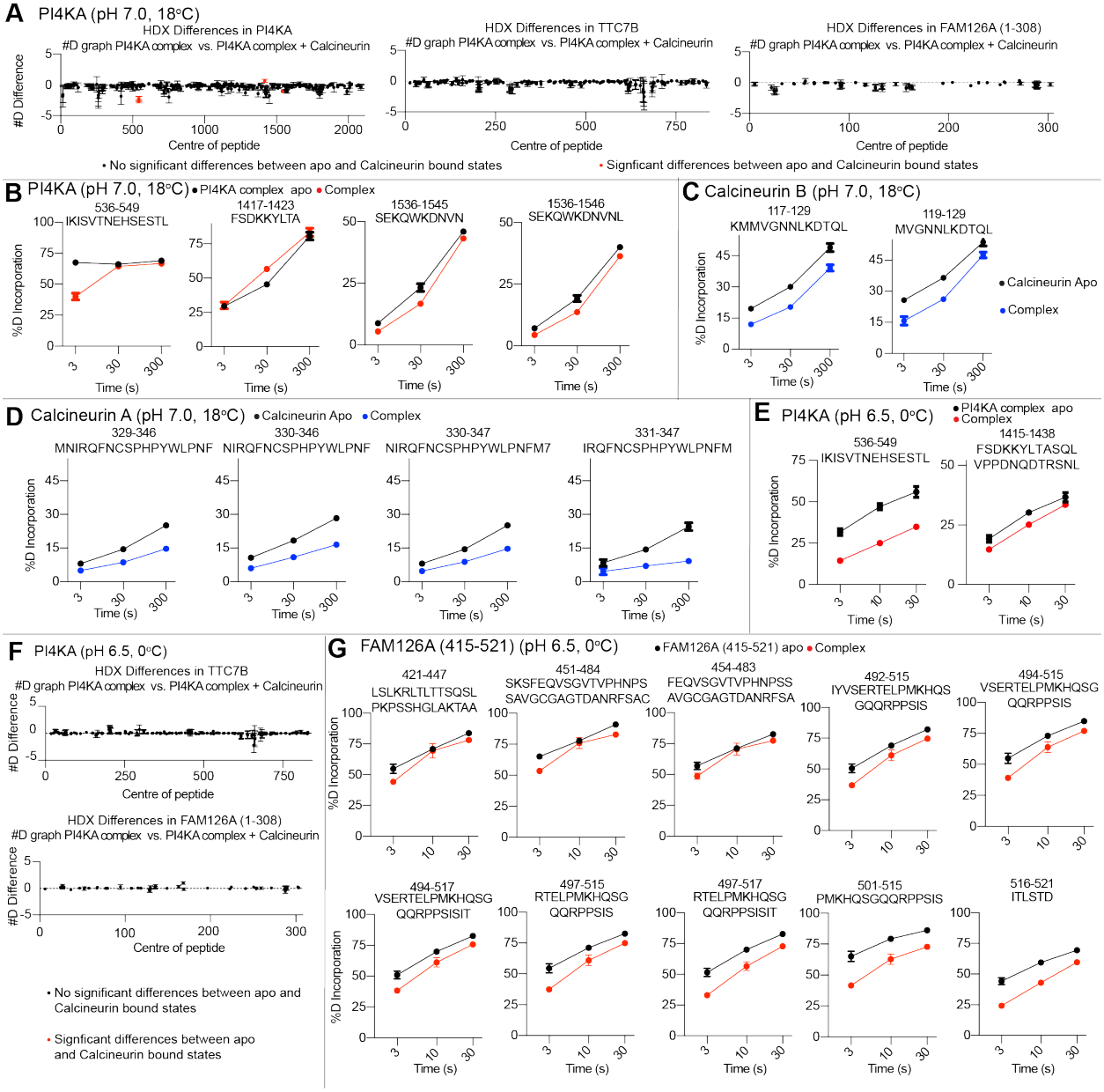

Supplemental Figure 4. HDX-MS data underlying all experiments

A. Sum of the number of deuteron difference of (L) PI4KA, (M) TTC7B, and (R) FAM126A (1-308) upon complex formation with Calcineurin analysed over the entire deuterium exchange time course (pH 7.0, 18°C). Each point is representative of the centre residue of an individual peptide. Peptides that met the significance criteria (see panels **B**) are colored red. Error is shown as standard deviation (SD) (n=3). The full source data underlying all HDX-MS data is included as an excel file.

B. Selected deuterium exchange time courses of PI4KA peptides (pH 7.0, 18°C) that showed significant (defined as >5% 0.45 Da, and p>0.01 in an unpaired two-tailed t test at any time point) changes in exchange. Error is shown as standard deviation (SD) (n=3).

C. Selected deuterium exchange time courses of Calcineurin B peptides (pH 7.0, 18°C) that showed significant (defined as >5% 0.45 Da, and p>0.01 in an unpaired two-tailed t test at any time point) decreases in exchange. Error is shown as standard deviation (SD) (n=3).

D. Selected deuterium exchange time courses of Calcineurin A peptides (pH 7.0, 18°C) that showed significant (defined as >5% 0.45 Da, and p>0.01 in an unpaired two-tailed t test at any time point) decreases in exchange. Error is shown as standard deviation (SD) (n=3).

889 **E.** Selected deuterium exchange time courses of PI4KA peptides (pH 6.5, 0°C) that showed significant
890 (defined as >5% 0.45 Da, and p>0.01 in an unpaired two-tailed t test at any time point) decreases or
891 increases in exchange. Error is shown as standard deviation (SD) (n=3).
892 **F.** Sum of the number of deuteron difference of (L)TTC7B, and (R) FAM126A (1-308) upon complex
893 formation with Calcineurin analysed over the entire deuterium exchange time course (pH 6.5, 0°C). Each
894 point is representative of the centre residue of an individual peptide. Peptides that met the significance
895 criteria (see panels **E**) are colored red. Error is shown as standard deviation (SD) (n=3). The full source
896 data underlying all HDX-MS data is included as an excel file.
897 **G.** Selected deuterium exchange time courses FAM 126A (415-521) peptides (pH 6.5, 0°C) that showed
898 significant (defined as >5% 0.45 Da, and p>0.01 in an unpaired two-tailed t test at any time point) decreases
899 or increases in exchange. Error is shown as standard deviation (SD) (n=3).
900
901
902
903
904
905

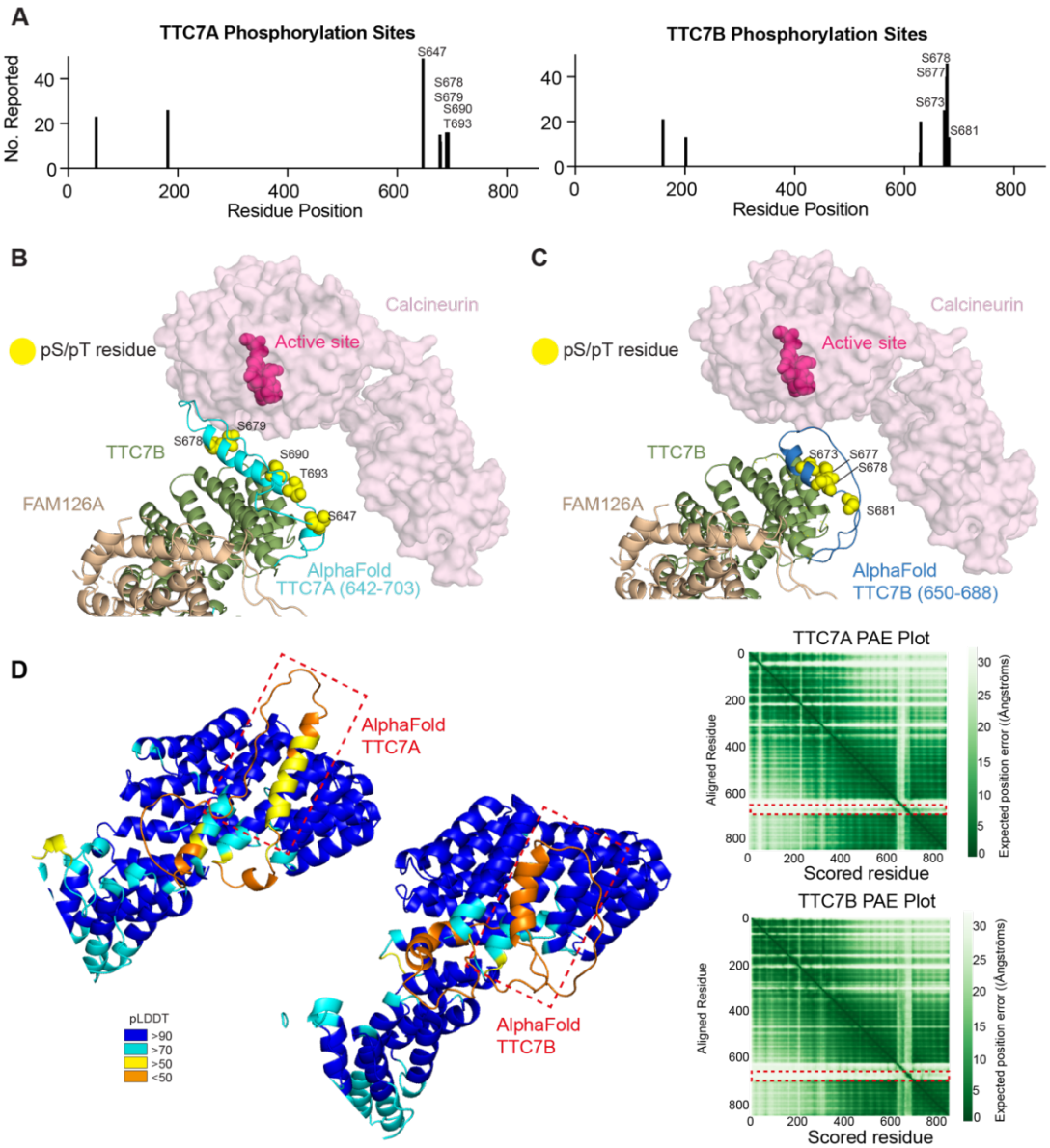

Supplemental Figure 5. AlphaFold modelling of TTC7A/B on cryo-EM structure reveals evolutionary conserved phosphorylation sites in TTC7A and TTC7B in close proximity to Calcineurin active site.
A. Phosphorylated serine/threonine residues in TTC7A (left) and TTC7B (right) reported on PhosphoSite (Hornbeck *et al*, 2015). Serine/threonine residues reported more than five times are shown.
B. Multiple reported TTC7A phosphorylation sites are in proximity to the Calcineurin active site. AlphaFold model of the disordered loop in TTC7A (642-703) is aligned to the experimental density for TTC7B. Threonine/serine residues reported to be phosphorylated are shown as yellow spheres. The AlphaFold model used for the alignment are shown in panel D.
C. Multiple reported TTC7B phosphorylation sites are in proximity to the Calcineurin active site. AlphaFold model of the disordered loop in TTC7B (650-688) is aligned to the experimental density for TTC7B. Threonine/serine residues reported to be phosphorylated are shown as yellow spheres. The AlphaFold model used for the alignment are shown in panel D.
D. (L) AlphaFold models of TTC7A and TTC7B coloured based on pLDDT according to the legend. The disordered loop not present in the experimental structure is boxed in red. The predicted alignment error (PAE) for both AlphaFold models are shown, with the areas boxed in red indicating the disordered loop in close proximity to Calcineurin in the PI4KA-TTC7-FAM126-Calcineurin structure.